

Characterization of the SiPM arrays for the JEDI polarimeter using a dedicated measurement setup

Anoop Nagesh Koushik
376121

Physics Institute III B
RWTH Aachen University

Submitted in partial fulfilment of the requirements for the degree of
Master of Science in Department of Physics,
Faculty of Mathematics,
Computer Science and Natural Sciences
RWTH Aachen University

December 2020

Supervisor: Prof. Dr. Jörg Pretz
Co-supervisor: Prof. Dr. Achim Stahl

Contents

1	Introduction	5
2	Physics Motivation	7
2.1	Baryon Asymmetry	7
2.2	Electric Dipole Moment – EDM	7
3	Instrumentation / Experimental equipment	9
3.1	Cooler Synchrotron – COSY	9
3.2	JULIC Cyclotron	10
3.3	JEDI Polarimeter – JePo	10
3.4	Silicon Photomultipliers – SiPM	12
3.4.1	Noise in the SiPM	13
3.4.2	Radiation Damage in Silicon	15
4	Irradiation of SiPM	17
4.1	Unexpected irradiation of SiPM at COSY	17
4.2	Annealing of SiPM	17
4.3	Irradiation of SiPM at Cyclotron	19
4.3.1	Preparation and design	20
4.3.2	Experiment	22
4.4	Automatized dark current characterization of the SiPM	25
4.4.1	Design	25
4.4.2	Measurements	30
4.4.3	Report generation with comparison	31
4.4.4	Faults	31
5	Characterization of SiPM Arrays	33
5.1	Design	33
5.1.1	Configuration of the instrument	33
5.1.2	Characterization of LED and reference SiPM	35
5.1.3	Angular absorbance of SiPM array	38
5.1.4	Illumination module	39
5.2	Measurements	41
5.3	Reports	42
6	Summary and Outlook	45
	Appendices	47
A	SiPM 161123-46 Report	47
B	SiPM 161123-07 Report	49

Chapter 1

Introduction

We live in a high matter concentration universe where matter-antimatter asymmetry exists possibly due to the Electric Dipole Moment (EDM). The Jülich Electric Dipole moment Investigation (JEDI) collaboration aims to directly measure the EDM of protons and deuterons where the CP violations occur, which in turn result in the matter-antimatter asymmetry. The experiments are being conducted with proton and deuteron beams in the storage ring at COoler SYnchrotron (COSY) Forschungszentrum Jülich, Germany. RF Wien filter is used to build-up polarization which is proportional to EDM, and a polarimeter to observe the polarization of the products of the scattering process of the deuteron beam on a carbon target. This polarimeter consists of scintillating crystals which emit photons. Instead of the traditional photomultiplier vacuum tubes (PMTs), Silicon-photomultipliers (SiPMs) are used instead, for their convenience, low operating voltage and for the fact that silicon detectors doesn't influence the polarized beam either with strong electric or magnetic fields.

During beam based alignment in 2019, an accidental irradiation of the SiPMs occurred. The damage imparted by the radiation resulted in a high dark current. To understand the extent of the damage, it was necessary to study the dark current and responsivity in the array of SiPMs. Hence independent measurement set-ups were constructed with a dedicated software for each of them to control and run the measurements.

Dark current measurement set-up was constructed to study the voltage dependence of the dark current for each SiPM in the 8x8 array. Data was analysed by the software (written in Python 3 and ROOT) after the measurement, providing a report on the SiPM array. Similarly, the responsivity measurement set-up was constructed where each SiPM in the array is illuminated, the resulting signal was recorded from the array and it is normalized with a reference SiPM signal to obtain the relative responsivity/charge. A similar report is generated in this case as well. Furthermore, the technique of annealing was utilized to reduce the radiation damage. Therefore, measurements were conducted again to study the annealing effects.

These dedicated measurement set-ups help us to sort out the better SiPM arrays from the ones which are damaged, so that the former can be used in the JEDI polarimeter detector again for the upcoming beam times.

Chapter 2

Physics Motivation

2.1 Baryon Asymmetry

Looking into today's universe, in which all of the Earth, the Sun and the galaxies seem to consist only of matter, the existence of a high matter-antimatter asymmetry resulting at a fundamental level seems to be obvious. But from the laws of nature, as of today, predict only a slight asymmetry with respect to matter and antimatter from CP violation (Charge-parity violation), which is found to be very small.

The ratio of matter to antimatter can be written as follows, with n_B as the concentration of baryons and \bar{n}_B as the concentration of anti-baryons and n_γ as the number of photons

$$\eta = \frac{n_B - \bar{n}_B}{n_B + \bar{n}_B} \approx \frac{n_B - \bar{n}_B}{n_\gamma} \quad (2.1)$$

According to the Big Bang theory[1], the Universe was very dense and hot at the time of its creation, implying the presence of equal amount of both matter and antimatter. Hence asymmetry should have occurred during the early stages of the Universe expansion, in a process called as Baryogenesis, in which matter and their antimatter eventually annihilated to photons and neutrinos leaving only a small amount matter which gave rise to the matter we see today.

It has remained as a challenge to understand the origin on this asymmetry, since the Standard Model (SM) of elementary particle physics failed to provide a satisfactory explanation and a wonderful motivation to go in search of new physics beyond the Standard Model[2].

2.2 Electric Dipole Moment – EDM

In 1967, *Andrei Sakharov* defined three conditions that have to be fulfilled in order to explain the matter-antimatter asymmetry[3]:

- Baryon number violation: The conservation of baryon number must be strongly violated in the early evolution of the universe.
- C and CP violation: If C and CP symmetries were to be conserved then the probability of a process creating a particle and another process creating its antiparticle should be the same, therefore conserving the baryon number.
- Deviation from thermal equilibrium: The moment when baryon number was generated, the universe was not in thermal equilibrium otherwise it is impossible for a system to violate baryon number.

Though the SM does accommodate CP violations via the phase in the Cabibbo-Kobayashi-Maskawa (CKM) matrix, it only fulfills these requirements up to a certain extent, but the resulting CP violation ($\eta \approx 10^{-18}$ [3]) is still too small to account for the observed baryon asymmetry ($\eta \approx 10^{-10}$ [4]). This opens up the search for finding the different sources of CP violation. The SM also falls short of explaining neutrino oscillations, baryogenesis rate as well as electric dipole moment (EDM).

In the framework of quantum mechanics, the EDM of a fundamental particle is defined with a spin, in order to retain the vector nature of the EDM. The magnetic dipole moment (MDM) of a particle is also defined with the same spin factor. This spin factor defines the direction inside the elementary particle. Under P (parity) transformation, only electric field is inverted and under T (time reversal) transformations only magnetic field is inverted. Therefore, the Hamiltonian of the system after applying both these transformations does not return to the original state, hence violating the CP symmetry[5].

This makes the EDM an interesting candidate as it is a necessary condition, according to the Sakharov's second condition. The SM predicts the EDM to be very small or even zero but the recent measurement of neutron EDM was found to have an upper limit of $1.8 \cdot 10^{-26} e \text{ cm}$ (90% C.L.)[6]. No direct measurement for the EDM of a charged hadron has been performed yet. This serves as a motivation to measure EDM for charged hadron.

Chapter 3

Instrumentation / Experimental equipment

3.1 Cooler Synchrotron – COSY

The COoler SYnchrotron - COSY, is a particle accelerator located at Forschungszentrum Jülich, Germany. It is designed to generate polarized and unpolarized proton beams in the medium energy range of 45 and 2700 MeV. Additionally, it can also provide deuteron beams between 90 and 2100 MeV. Beam cooling is also developed for an improved beam quality at this facility[7].

The main components of COSY include:

- The Source for the production of polarized and unpolarized Hydrogen and Deuterium ion beams
- Jülich Isochronous Synchrotron (JULIC) also called the injection cyclotron for pre-acceleration of the ion beams
- Main storage ring - COSY for accelerating the beams up to a momentum of 3.7 GeV/c

The beams produced by the source are transferred into the injector cyclotron JULIC (Jülich Isochronous Cyclotron) which accelerates the ion beam to kinetic energies up to 45 MeV for Hydrogen beams and up to 76 MeV for Deuteron beams. These are then transferred via an injection beam line into the main storage ring COSY. The injection beam line accommodates a small polarimeter known as the Low Energy Polarimeter (LEP), that can measure the polarization of the beam. Before injection into the main ring, the two electrons from the atoms are removed by a stripping reaction in a thin carbon foil resulting in proton/deuteron beam.

The COSY storage ring is shown in Figure: 3.1. The accelerator ring has a circumference of 184 m. Two straight sections with a length of 40 m along with the two arc sections with a radius of 16.5 m form the accelerator. Normal-conducting water cooled dipole magnets that can reach magnetic fields up to 1.58 T, bend the beams in the arc sections. Additionally, quadrupole and sextupole magnets are incorporated throughout the ring to focus and correct chromaticity effects respectively. The cooling of beams is a distinctive feature of COSY. This is achieved by elastic cooling and/or stochastic cooling. As shown in the figure, two coolers are placed in the straight sections, where the beam positions are sampled in the form of small packages.

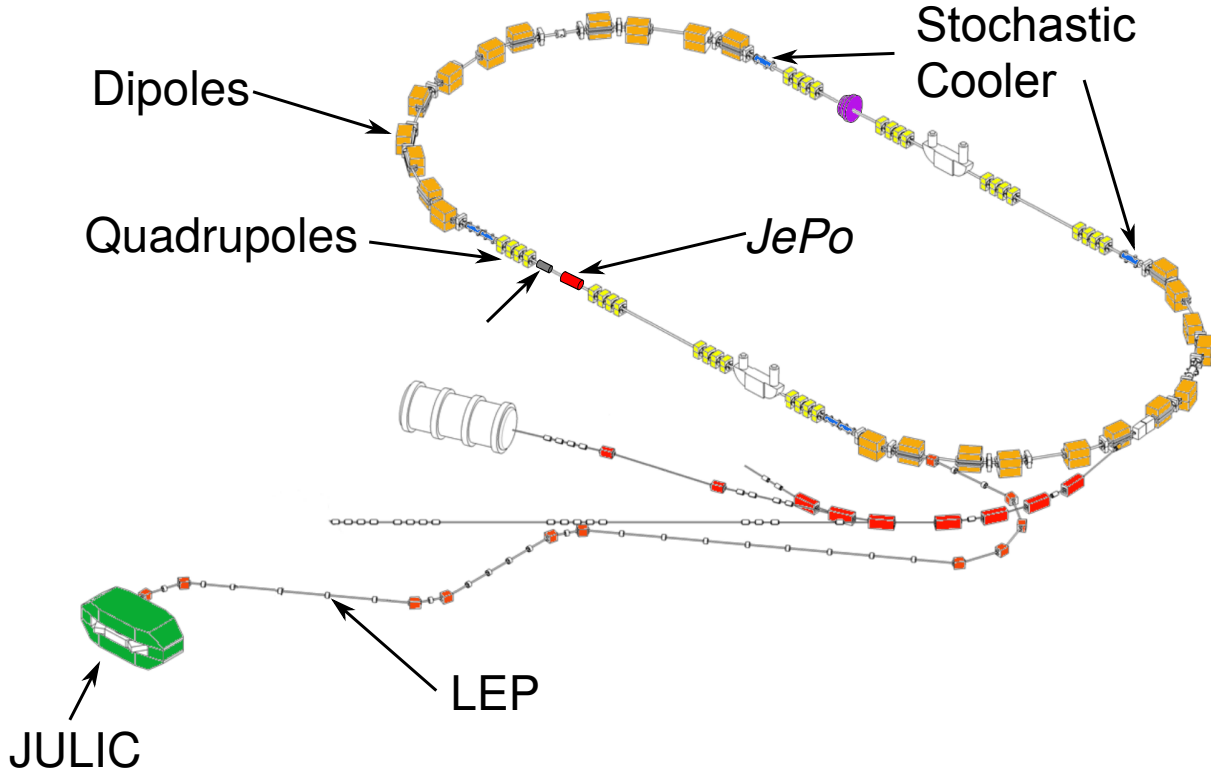


Figure 3.1: Cooler Synchrotron (COSY) at Forschungszentrum Jülich

3.2 JULIC Cyclotron

The Jülich Light Ion Cyclotron (JULIC) (see Figure: 3.2) was commissioned in the year 1992. It is an intermediate energy cyclotron used as the injector for COSY. In the initial years H_2^+ -beams were used for stripping injection into the synchrotron ring, with a 2.45 GHz[8] microwave source. Later, it was modified to deliver polarized H^- or D^- beams within the acceptance of the cyclotron during 10 - 20 ms[8] of the injection period of COSY. The cyclotron was also equipped with a target behind the septum which provides fast exchange of target constructions. The irradiation is achieved with 45 MeV protons and 76 MeV deuterons[9]. It is also equipped with various dosimetry systems such as PTW[®] Farmer ionization chambers, PTW[®] Bragg Peak chambers, Gafchromic[®] Dose sensitive foils to monitor and control ongoing radiation.

Since the experiment for surface target is performed in air, it is kept 1.8 m away from the end of the pipe, with 1 mm aluminum foil in-between to reduce the protons energy to 35 MeV[9]. The rate of irradiation used for the experiment in this thesis are 1 mG/s and 3 mG/s.

3.3 JEDI Polarimeter – JePo

An important requirement for the successful search of the Electric Dipole Moments using Storage Rings (srEDM) is to find a way to determine the change in polarization direction during beam store with high sensitivity ($<10^{-5}$ [10]). Since the magnetic field cannot be used because of its effects on the spin motion via the magnetic dipole moment (MDM), another method was required to determine the particle energy. A LYSO:Ce (Cerium-doped lutetium yttrium oxyorthosilicate) scintillating crystal was used for this purpose. It is dense (7.1 g/cm^3), radiation hard along with small decay time of 41 ns[5] which makes it a good

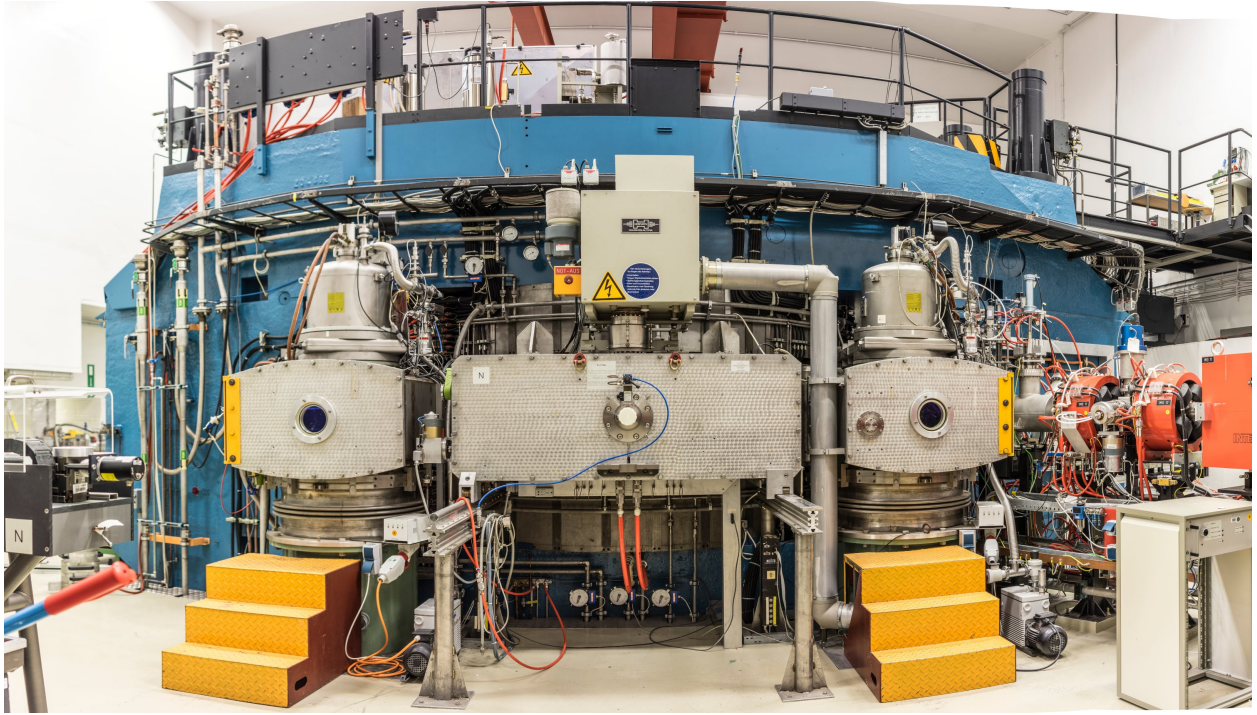


Figure 3.2: Jülich Light Ion Cyclotron (JULIC) in Cooler Synchrotron (COSY) at Forschungszentrum Jülich

scintillating material.

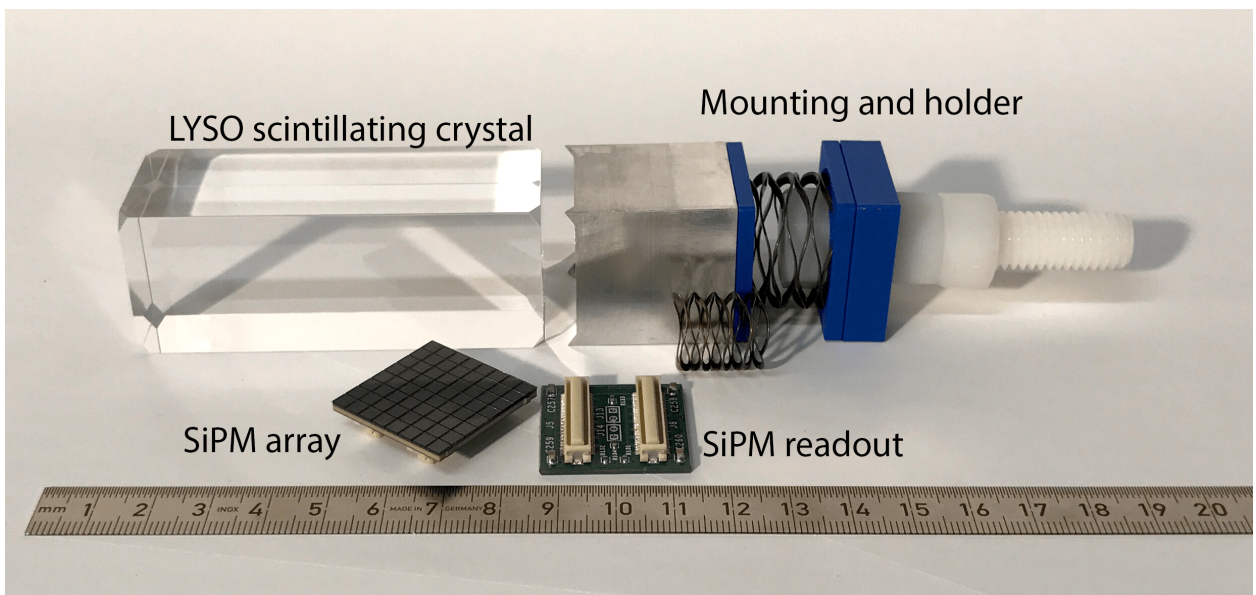


Figure 3.3: A unit of ΔE detector in JEDI polarimeter - LYSO crystal, SiPM array along its readout and mounting case and the holder

Jülich Electric Dipole moment Investigations (JEDI) polarimeter, was therefore constructed in the straight section of COSY ring, see Figure: 3.4. Each unit consists of a segmented calorimeter made of LYSO crystals, silicon photomultipliers (SiPMs), SiPM readout, and a 2 cm thick plastic scintillator for particle identification[5] (see Figure: 3.3). A carbon target was used for proton or deuteron scattering. The polarimeter, consisting of 52 units, occupies 1.3 m space. 48 of these units were arranged in 4x3 arrays along the four directions radiating out from the center and the remaining four of these units are placed diagonally

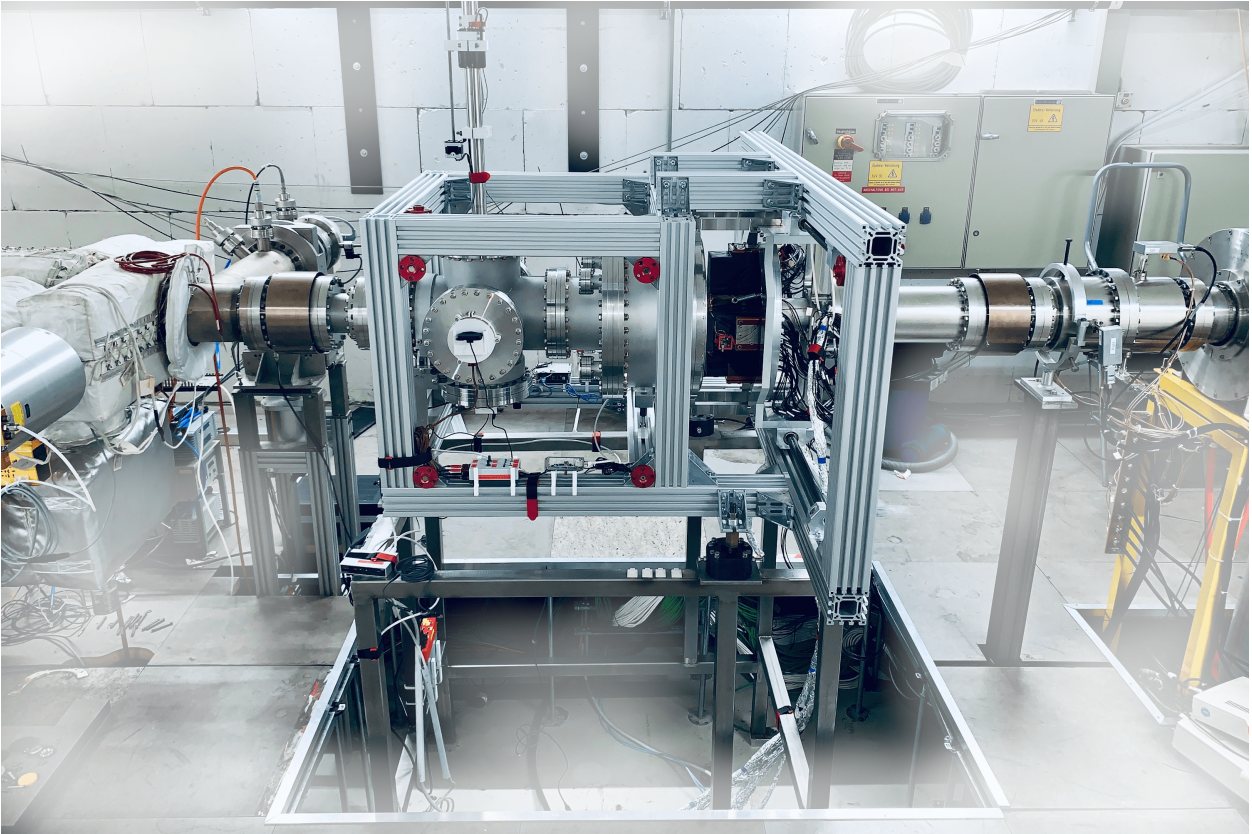


Figure 3.4: JEDI polarimeter in COSY

opposite to the four vertices of the center. The resulting arrangement is shown in Figure: 3.5. With this arrangement we can effectively measure left, right, up and down directions asymmetry when the polarized beam is accelerated.

3.4 Silicon Photomultipliers – SiPM

The silicon photomultiplier (SiPM) is a solid state photodetector composed of several hundreds to thousands of single-photon avalanche diodes (SPADs), typically $10 - 50 \mu\text{m}$ in size, called microcells or pixels[11][12]. Each of them is connected in parallel to the read out circuit with their own quenching resistor. These SPADs are operated in Geiger mode.

Geiger mode: A free charge carrier created or drifting in high electric field in the depletion region is accelerated such that it carries sufficient kinetic energy to create a diverging avalanche of electrons and holes, via impact ionisation. The APDs are in reverse voltage bias above the breakdown voltage to set it on Geiger mode.

The incidence of a photon on the SPAD, generates a large electric signal due to breakdown as it is being operated in Geiger mode. It is possible to count each microcell triggered separately because the signal is the sum of all triggered SPADs[11]. The SiPM operates at a low supply voltage (as low as 27 V), is robust, compact and insensitive to magnetic field which makes it an excellent choice for replacement of traditional photomultiplier tube (PMT) (requires very high voltage, greater than 1000 V).

In JEDI polarimeter, these SiPMs replace the PMT's. They are coupled with the LYSO crystal. When photons are generated in the crystal, the signal proportional to the energy deposited in the crystal is produced.

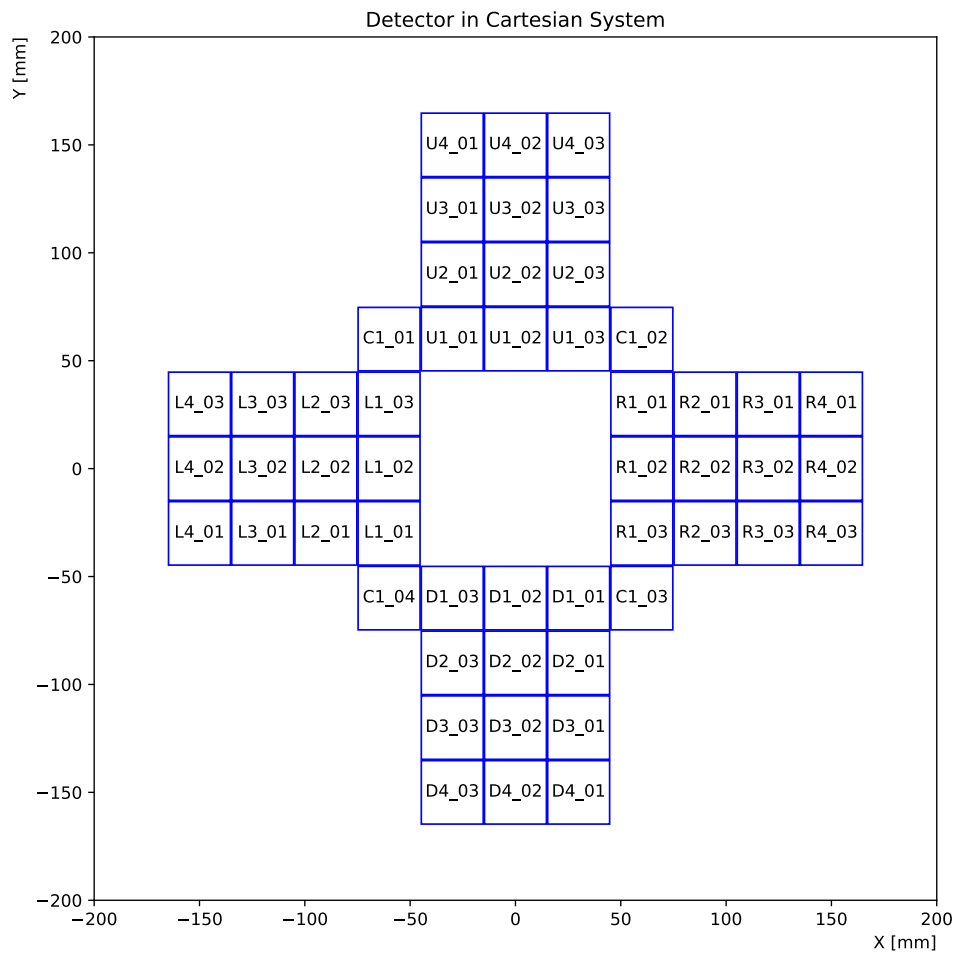


Figure 3.5: The arrangement of the ΔE detectors in JEDI polarimeter[5]

In this thesis, all the SiPMs that were analysed and characterized were SensL J-Series 30020 model.¹

3.4.1 Noise in the SiPM

Noise in the photo devices obeys Poisson distribution in the absence of photons. There are several factors affecting the noise in the SiPM. Some of them are: thermal noise and dark current / dark noise / dark count rate.

- Thermal noise: also known as Johnson noise or white noise, is the noise generated in the device due to the fluctuations in the voltage across a dissipative circuit such as resistors caused by thermal motion of the charged carriers. The current generated due to thermal noise is given by:

$$I = I_0 \exp\left(\frac{\Delta E \cdot q}{k_B T}\right),$$

where k_B is the Boltzmann constant, q is the charge and T is the absolute temperature.

- Dark noise: The false positive triggers of the microcells in the complete absence of the photon. This is primarily due to thermal electrons generated in the active volume and

¹Note: **SensL Technologies Ltd.** was acquired by **ON Semiconductor** in May 2018. Hereafter for simplicity, "SensL" will be used in the places to refer to this company which is now ON Semiconductor as it is easy to relate to the print on the modules.

the defects in the device. These defects and thermal electrons trigger the avalanche in high field region. This noise signal is identical to the signal generated by a photon and we consider this, only in the absence of photons[13][12]. Since the amplitude of the noise signal is similar to that of a single microcell, while an actual signal involves triggering of multiple microcells, the noise can be neglected in the presence of a signal.

3.4.1.1 Temperature dependence of dark current

Breakdown voltage and dark noise are a function of the temperature. The breakdown voltage is a linear function of temperature (see left panel of Figure: 3.6). For the devices used in this thesis, the change in breakdown voltage is as small as $21.5 \text{ mV}/^\circ\text{C}$ [12].

Unlike breakdown voltage, dark noise is rather an exponential function of temperature (see right panel of Figure: 3.6), which results in much higher noise levels with small increase in temperature. The dark current measurement is accompanied by heat generation and therefore, an algorithm was used to bypass this issue allowing enough time for heat to dissipate from the SiPM which is discussed in Section: 4.4.1.3. An example provided by SensL states that, for every 10°C reduction in device temperature, there is a 50% decrease in the dark count rate. The provider also recommends the usage of active cooling if the temperature fluctuations are larger.

In JePo, SiPMs are attached to a large crystal which stabilizes temperatures by stabilizing tunnel air temperature of COSY. This limits the temperature variations within a degree Celsius, which are recorded using a digital thermometer incorporated in the housing. For this work, we did not have to deal with temperatures fluctuations since the lab temperatures were controlled through air conditioning. Moreover, an active cooling results in an electromagnetic interference with the setup.

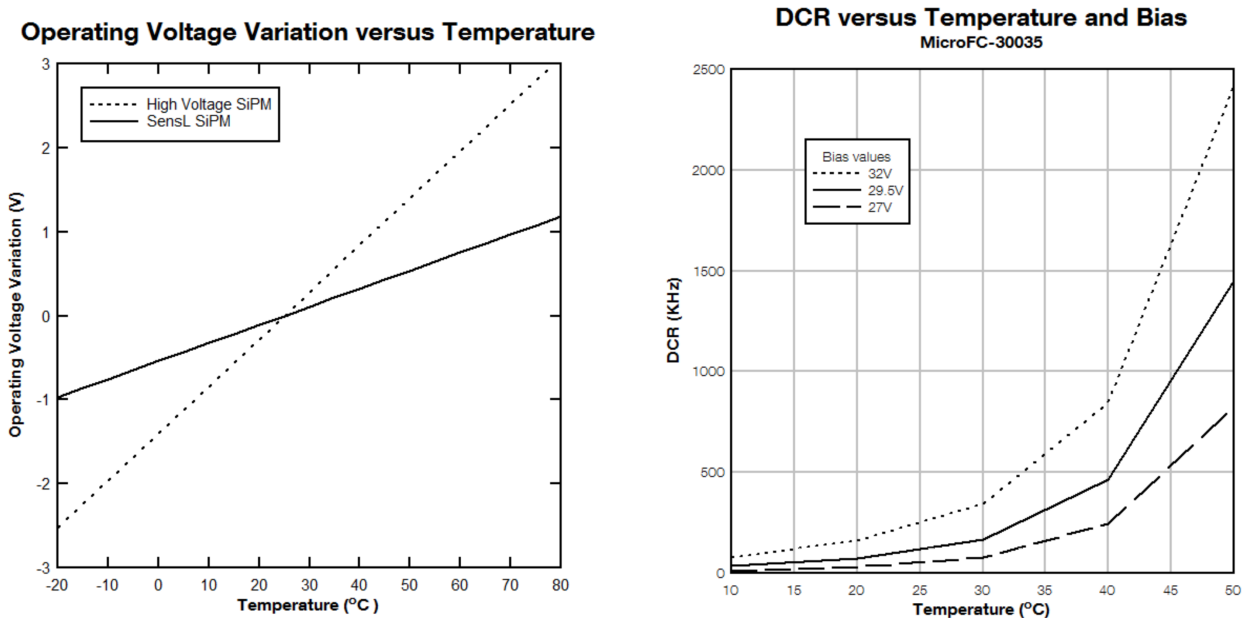


Figure 3.6: Temperature dependence of operating voltage and dark count rate[12]

3.4.1.2 Photon Detection Efficiency (PDE) and Responsivity

Photon Detection Efficiency (PDE) can be defined as the ratio of the number of detectable photoelectrons to the number of photons incident on the SiPM. PDE is also a function of

the wavelength of the incident light, the applied overvoltage² and microcell fill factor. This is slightly different from quantum efficiency³ since this is a statistical probability of photon triggering the microcells.

$$PDE(\lambda, V) = \eta(\lambda) \cdot \epsilon(V) \cdot F,$$

where $\eta(\lambda)$ is the quantum efficiency of silicon for a given wavelength, $\epsilon(V)$ is the avalanche initiation probability and F is the fill factor of the device.

Responsivity is the average photocurrent produced per unit optical power, which is given by:

$$R = \frac{I_p}{P_{op}},$$

where I_p is the measured photocurrent and P_{op} is the incident optical power at a particular wavelength over the sensor area.

In the measurement of responsivity, low intensity light pulses should be used, which ensures that the sensor is not saturated. Additionally, it requires an accurate reference sensor. The measurement for saturation of the SiPM is discussed in the Section: 5.1.2.2

3.4.2 Radiation Damage in Silicon

In this section we discuss the effects of radiation on silicon detectors. The defects caused due to radiation can be categorized into 2 parts: Bulk damage and Surface damage.

Bulk damage When an incoming particle, hadrons (protons, neutron etc.) or high energy leptons, transfers certain amount of energy to the atom, where the energy is greater than the binding energy of the Si atom (~ 25 eV[14]), the atom (Primary Knock-on Atom (PKA)) is displaced in the lattice inducing interstitial defect and vacancy (Frenkel defect). If the energy of PKA is sufficiently large, it can displace additional atoms resulting in cluster defect. Depending on the incoming particle type and its energy, the number of crystal defects produced is typically assumed to be proportional Non Ionizing Energy Loss (NIEL) hypothesis[15]. This leads to the concept of radiation hardness factor.

Surface damage When the silicon detectors are exposed to low energy x-rays, surface damage occurs which affects the interface layers and oxides.

Surface damages are permanent while bulk damage can be reduced to a certain extent. Interstitials and vacancies can move inside the crystal lattice and are very mobile at high temperatures. Interstitials and vacancies may annihilate each other or diffuse out of the surface reducing the defect over a period of time[16]. These are sped up at high temperatures for a certain duration of time and is called as annealing which is discussed in detail in the Section: 4.2.

Radiation damages result in an increase of leakage current (dark current), decrease of signal and change in the effective doping density[16]. This requires us to compensate for the damage which causes deviations from the ideal behaviour.

²Overvoltage is the difference of reverse biased voltage to the breakdown voltage

³The quantum efficiency is a measure of the likelihood of an incident photon creating an electron-hole pair in the sensitive volume of the sensor.

Chapter 4

Irradiation of SiPM

4.1 Unexpected irradiation of SiPM at COSY

During the beam based alignment at COSY in the winter of 2019, an accidental irradiation of the SiPM took place where the SiPMs were exposed to high intensity gamma radiation. This was caused by the activation of the beam pipe at one of the exit windows when the beam was being moved to the extreme distances from the beam pipe center. This window is located at the JEDI polarimeter. The dosage rate of this exposure was measured to be $35.9 \mu\text{Sv/h}$.

Since SiPMs are not completely radiation hard (see Section: 3.4.2, this lead to damage in a few SiPM modules. Figure: 4.1 shows the dark current reading for the damaged SiPMs, radially from the center of the beam pipe, where the values are larger than for the outermost SiPMs. This motivated us to conduct an investigation for the radiation damage on the SiPM and consequently finding methods to reduce these damages.

4.2 Annealing of SiPM

The primary cause for the damage of the SiPM by the radiation, is the creation of vacancies and interstitial defects (see Section: 3.4.2). These vacancies and interstitials are mobile, and can diffuse very fast at high temperatures. It is possible that during this motion, the interstitials may annihilate the vacancies at a regular position, thereby compensating the defect. This effect can be facilitated by the process of annealing. Moreover, the displaced atoms can also combine with other kinds of defects, forming stable secondary defects[14]. This can be achieved by two kinds of annealing:

- High-temperature thermal annealing: The material is placed in an oven at high temperature for a certain duration, and is then slowly lowered to room temperature in small steps.
- Room-temperature self-annealing: The material is kept undisturbed at the room temperature for a very long duration.

To treat the defects arising from the irradiation, three irradiated SiPM's were subjected to high temperature thermal annealing for different time intervals and in different batches. A significant decrease in the dark current was observed, thus indicating defect-compensation, in each annealing session. However, this reduction gradually decreased with the annealing time and reached a saturation. In this thesis, we discuss our observation and results for one of the SiPMs, namely SiPM 161123-07, since the conclusions with the other two are

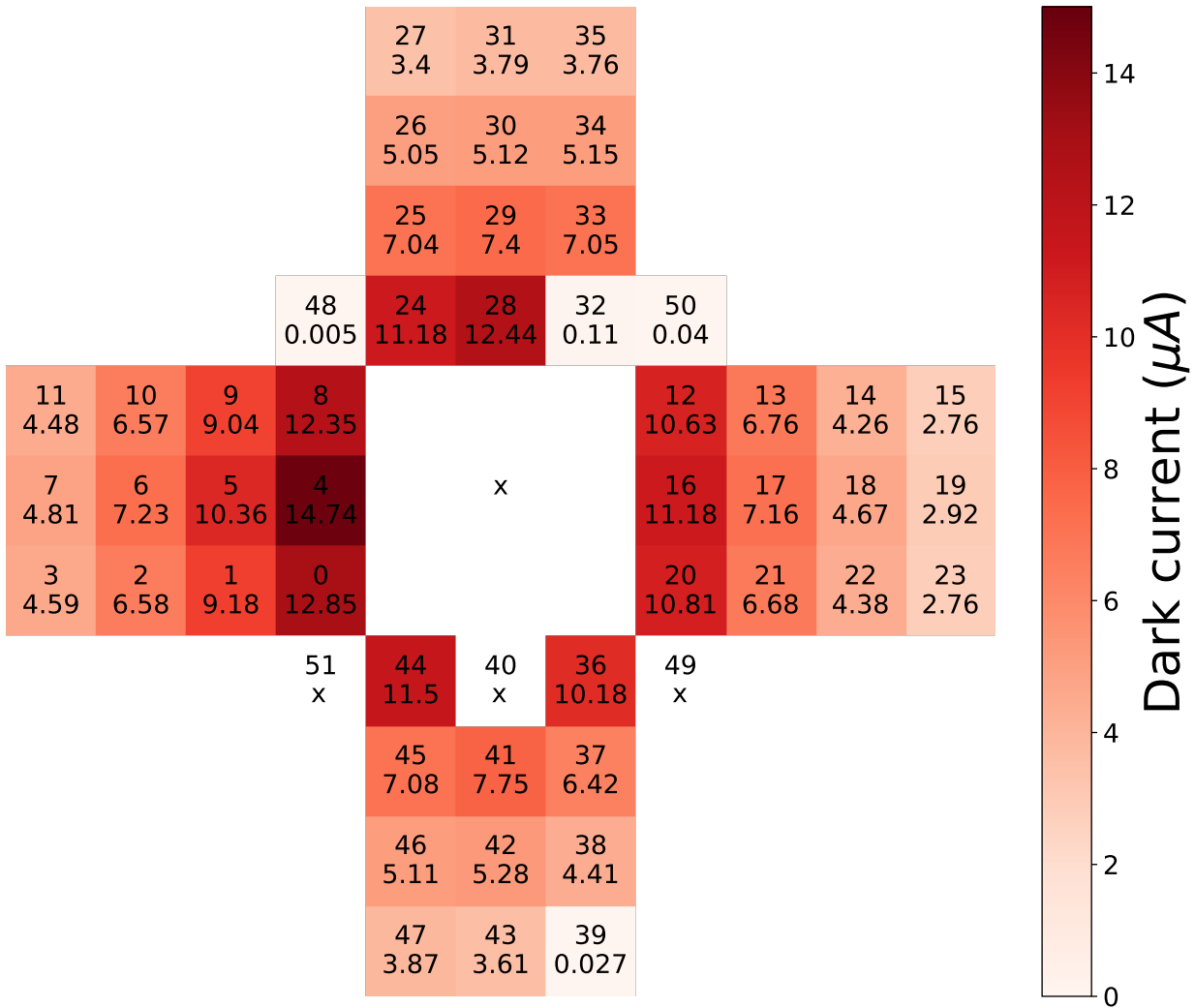


Figure 4.1: Dark current readings for the SiPMs in JePo as arranged in Figure: 3.5 on October 15, 2019, after the accidental irradiation. Center marked 'x' shows the beam pipe center. For each box, SiPM channel number is on the top with it's dark current in μA

the same. The higher dark current in the SiPM map was always closer to the beam pipe indicating higher radiation damage.

The sessions in which SiPM 161123-07 was thermally annealed are shown in Table: 4.1. At first, the SiPM was annealed at $120^{\circ}C$ for a initial sessions. Later, as learnt that the plastic connector could resist temperatures up to $170^{\circ}C$, the subsequent annealing procedures were performed at a higher temperature of $150^{\circ}C$.

A cross comparison of the dark current of the SiPM non-annealed versus maximally annealed, is shown in the Figure: 4.2. A dark current measurement was performed before annealing. The first session of annealing was done at $120^{\circ}C$ for 20 h with 40 min of cooling. Comparing the dark current data before annealing, with the dark current data after annealing of 20 h, as shown in Figure: 4.2(a), we observed that there is an approximately 3.5 times decrease in the dark current. After few more sessions with $120^{\circ}C$, the temperature was increased to $150^{\circ}C$ which resulted in a sharp decrease in the dark current. Figure: 4.2(b) shows that the reduction in the dark current is approximately 24 times after it was annealed for 266 h in comparison to a non-annealed SiPM.

In Figure: 4.2(c), one can see that the relative reduction in the dark current between the 243 h and 266 h of annealing, is close to 1, that implies that the reduction in the dark current

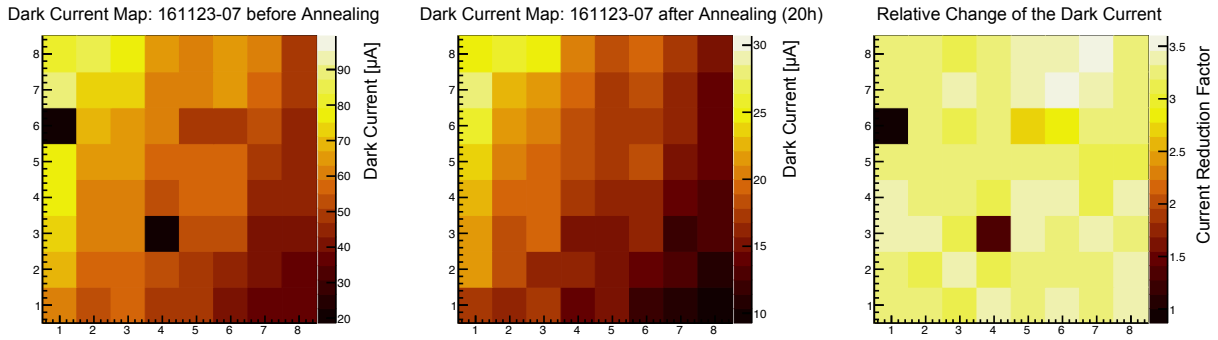


Figure 4.2(a): First annealing session at 120°C for 20 h. Reduction in dark current is approximately 3.5 times.

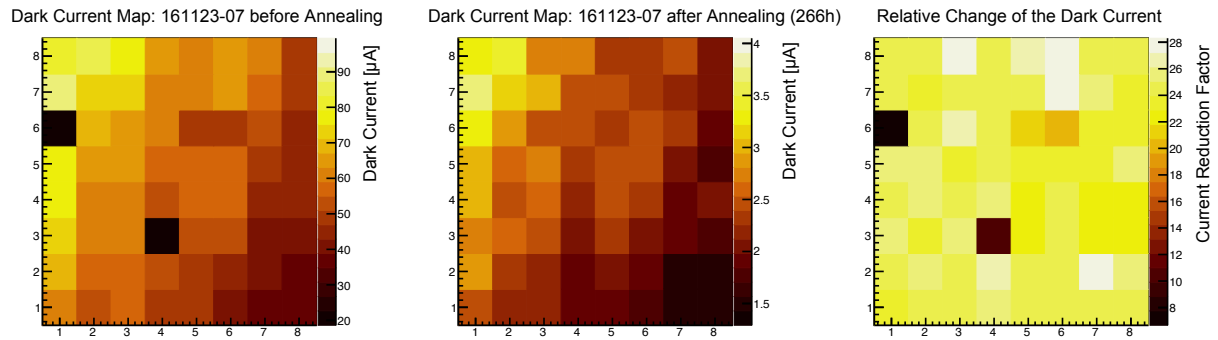


Figure 4.2(b): Last annealing session at 150°C (total of 266 h) in comparison with non-annealed data. Reduction in dark current is approximately 24 times.

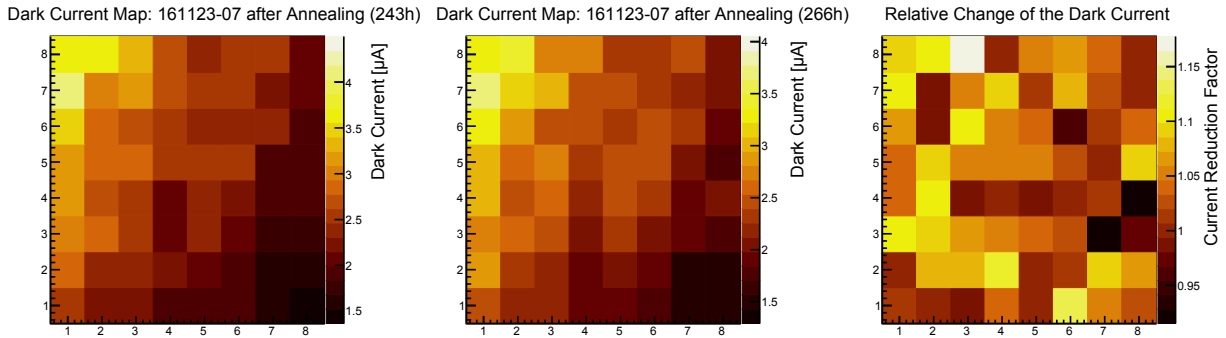


Figure 4.2(c): Last annealing session at 150°C for 23 h. Comparison with the previous session. Reduction of dark current is almost negligible indicating saturation.

Figure 4.2: Comparison of dark current of thermally annealed SiPM 161123-07

has reached a saturation. Annealing further therefore was not expected to yield any further significant reduction in the dark current. A complete comparison of dark current reduction for each row of Table: 4.1 is shown in Figure: 4.2 can be found in Appendix: A.

4.3 Irradiation of SiPM at Cyclotron

To perform an in-depth study of the irradiation of an SiPM, we conducted a small experiment with a controlled radiation source - a cyclotron (JULIC, see Figure: 4.3), an SiPM connected to the measurement setup, and a DAQ software.

The DAQ recorded the dark current continuously (in both cases of radiation being on or off), while also recording the triggers of the radiation. The damage caused to the SiPM

Date	Temperature	Annealing time (h)	Total Annealing time (h)
15.10	120	20:00	20
16.10	120	20:00	40
17.10	120	20:00	60
18.10	120	20:00	80
21.10	120	61:00	141
22.10	150	24:00	165
23.10	150	24:00	189
24.10	150	15:00	204
25.10	150	15:00	219
26.10	150	24:00	243
27.10	150	23:00	266

Table 4.1: High-temperature annealing data for the SiPM 161123-07



Figure 4.3(a):

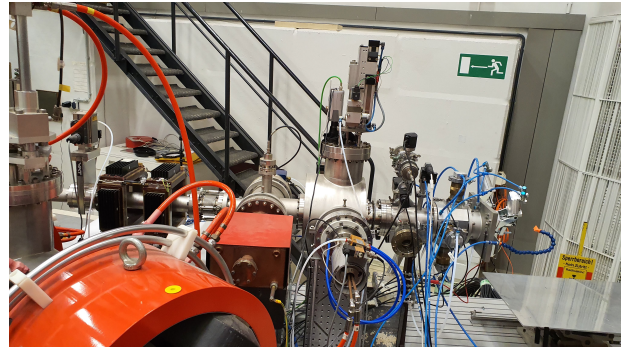


Figure 4.3(b):

Figure 4.3: (a) Location of the experiment - JULIC. (b) Experiment was placed at the end of the cyclotron ring.

during this experiment was similar to the accidental damage of SiPM in the second ring of COSY which is mentioned in Section: 4.1. Although the accidental event at COSY happened with a beam consisting of ~ 1 MeV protons, a beam with 45 MeV protons was used for this experiment.

4.3.1 Preparation and design

A special module was designed in OpenSCAD¹ to hold the SiPM array at an angle of 45° or parallel to the ground. The cap with an opening for the module was designed to cover the SiPM without obstructing the radiation. The CAD design of the module and the cap are shown in the Figure: 4.4(a), and its assembled unit in Figure: 4.4(b).

These CAD objects were 3D printed using Ultimaker 3. A black pigmented Polyvinyl fluoride (Tedlar[®]) was used to cover the opening of the cap to completely block visible light from falling on the SiPM [17]. The setup had two dosimeters next to the SiPM holders as shown in Figure: 4.5. Radiation film was also attached directly on the top of the SiPM array to observe the distribution of the radiation over each SiPM in the array, shown in Figure: 4.6(b). Another radiation film was placed on top the setup as shown in the Figure: 4.6(a).

The source of the radiation was JULIC (Section: 3.2) which provided the dosage readings. The measurement setup was designed to record the dark current along with the dosimeter

¹OpenSCAD is a script-only free software for creating solid 3D CAD (Computer Aided Design) objects

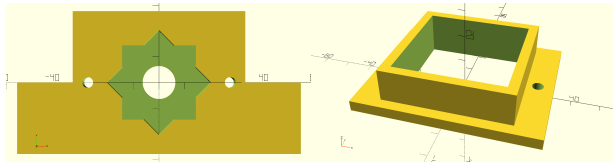


Figure 4.4(a):

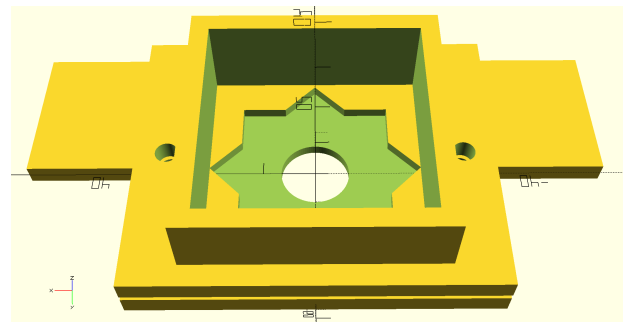


Figure 4.4(b):

Figure 4.4: (a) CAD object of the SiPM holder and the cap created in OpenSCAD. (b) CAD objects assembled into a single unit.

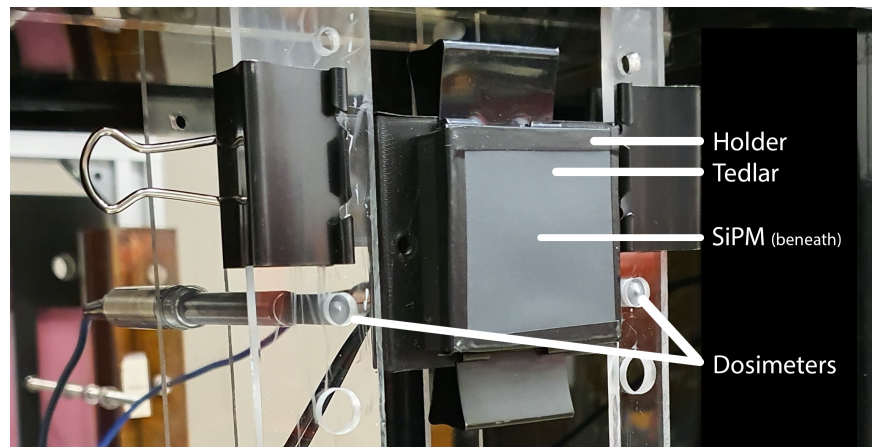


Figure 4.5: Experiment setup with Tedlar and dosimeters.

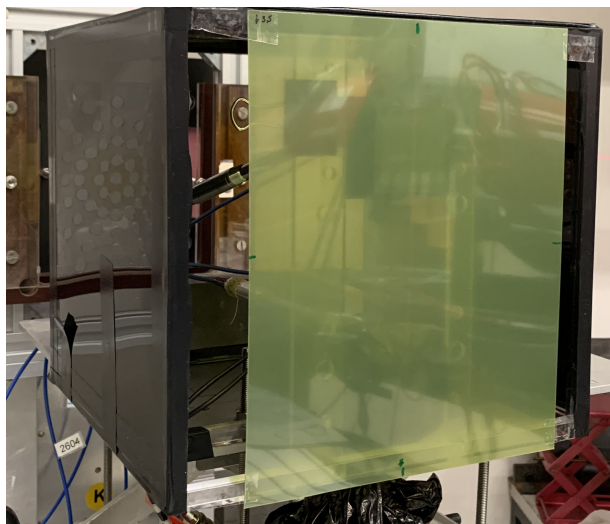


Figure 4.6(a):

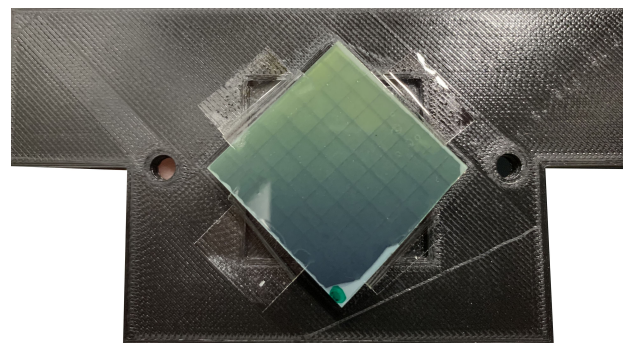


Figure 4.6(b):

Figure 4.6: (a) Radiation film was placed on the experiment to understand the distribution of the radiation. (b) Small radiation film was placed on the SiPM. The lower part had greater exposure to the radiation and hence the film is darker

readings. The current was measured with Fluke Pico-ammeter and data acquisition (DAQ) was running on Raspberry Pi. A live web server was set-up with an interface for plotting data in real-time. The change in the dark current due to radiation was very apparent when

the radiation was toggled. This was an added confirmation that the measurement setup was working as expected.

4.3.2 Experiment

This experiment was conducted over a span of 2 days. The SiPM array was at a reverse bias of 26 V. The time difference between the cyclotron computer and our DAQ was 22 s. The time interval between switching off the radiation and switching it back on, which is the data of our interest, was approximately 3 minutes. Over the 2 days, a total of 11 Gy radiation was radiated to the SiPM array at 2 different rates. On day 1, the total radiation dosage was 1 Gy at the rate of 1 mGy/s. On day 2, for a radiation dosage between 1 Gy and 2 Gy, the rate was 1 mGy/s, and for dosage up to 11 Gy, the rate was approximately 3 mGy/s.

The change in the dark current with respect to the radiation dosage is illustrated in Figure: 4.7. The total dark current of the SiPM array before the experiment was of the order of magnitude 1. After the radiation of up to 11 Gy, the total dark current was of the order of magnitude 3.

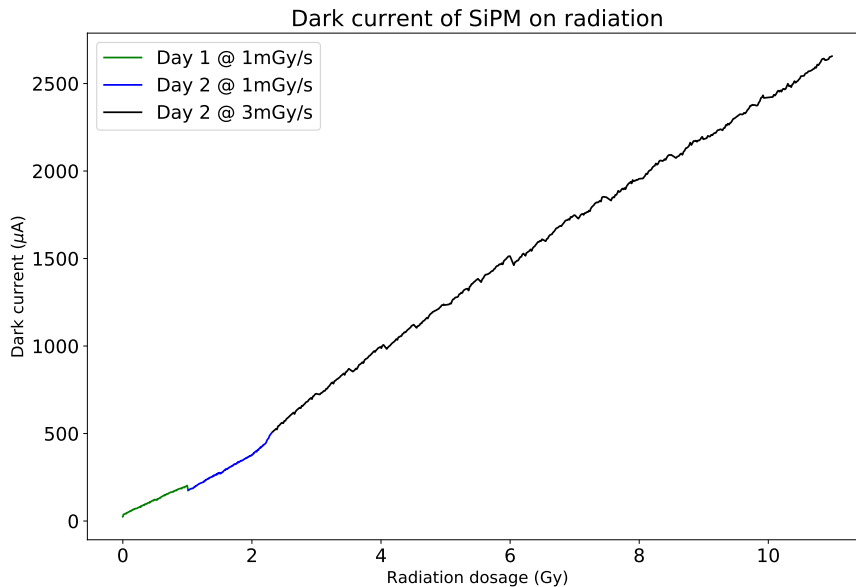


Figure 4.7: Dark current readings during the experiment when the radiation was off. Accumulative of both the days with different dosage rate.

The data points were averaged over the time window between the radiation being off and on, and plotted against the mean radiation dosage. A simple linear regression fit, as shown in the Figure: 4.8 with slope $\sim 0.24 \text{ mA/Gy}$, indicates that there is an increase in the dark current for every 1 Gy of radiation received.

After irradiation up to 11 Gy, we conducted a dark current SiPM by SiPM measurement in the array with SiPM developers board attached by multiplexers to route current from each channel of the board. They were further linked to each SiPM in the array developed by Dr. Fabian Müller during his PhD[5] in Institut für Kernphysik, Forschungszentrum Jülich in 2019. The dark current in the array is illustrated in Figure: 4.9. As explained in Section: 4.3.1, we set the SiPM at an angle, where the SiPM on the first row of the eighth column (SiPM 8) was pointing towards the center of the radiation beam. One can see a pattern in the increase of dark current near SiPM 8, which has much higher exposure to the radiating beam than the others. Additionally, the arc like pattern of dark current match with the arcs like pattern of the area exposed to the beam.

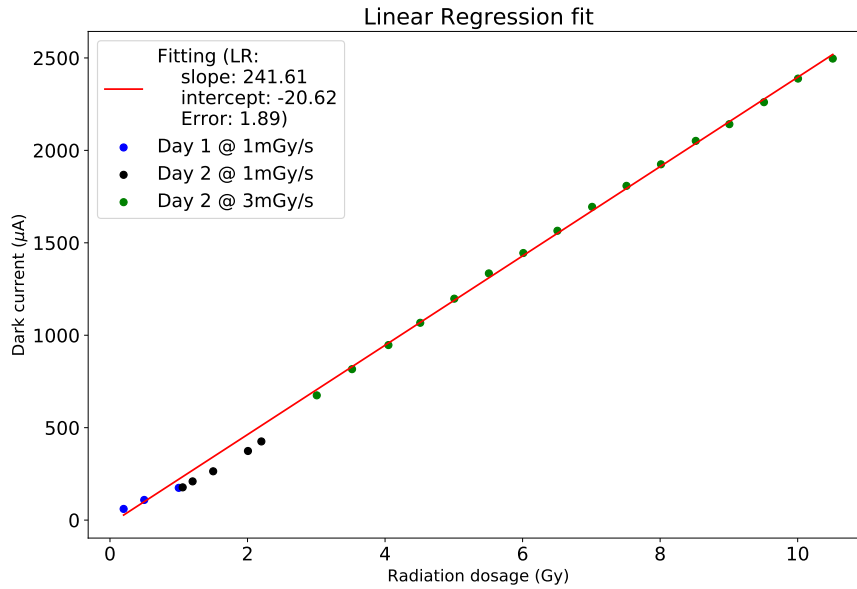


Figure 4.8: Linear Regression fit to the obtained data, only for the rate 3 mGy/s.

To study the self-annealing at room temperature over a long period of time, new measurements were taken 2 months after the experiment. There was a significant decrease in the dark current, but in comparison to high temperature annealing, as discussed in Section: 4.2, the overall reduction was rather small. Additionally, the time period for the reduction to saturate is significantly longer. Hence, high temperature annealing is better suited for re-usability.

The current-voltage (IV) plot for the SiPM array on 0 days and after 2 months for room-temperature self annealing is shown in Figure: 4.10, while Figure: 4.11 shows the dark current for each SiPM. Moreover Figure: 4.11 also shows the average dark current for each SiPM in array, as obtained from the fits in Figure: 4.10. These measurements were recorded and produced by an automatized dark current characterization setup discussed in Section: 4.4. One can see the decrease in dark current for each SiPM is rather small, but collectively it contributes significantly to the array. It was noted that there were few SiPMs whose damage was beyond what could be explained with the available data. One of the reasons for such an anomaly in the dark current could be the faulty jumps from the multiplexer channeling which will be discussed in the Section: 4.4.4.

To find the change in the trend because of self-annealing, the dark current measurements over 16 days were plotted against the voltage. The output voltage was changing due to the drift in the internal reference of the power supply unit. This drift is dependent on numerous factors, including temperature variation[18], which is shown in left panel of Figure: 4.12. On the right panel, we see the difference between the fitting for the dark current on 0 day (Figure: 4.10) from the data points of the left panel. The more negative these points are, the greater is the reduction in the dark current. This trend progresses as the number of days increase until saturation.

Figure: 4.1 shows the reduction in the dark current by room-temperature self annealing in the JePo, from the day it was accidentally irradiated, i.e. on October 15, 2019 (left panel), to a later measurement on January 22, 2020 (right panel).

This experiment gave us an insight on the damage caused by the radiation on SiPM array, the arc patterns, and the methods to reduce the dark current either by self-annealing at room temperature or annealing at high temperature. This enabled us to reuse the irradiated SiPM in the further experiments. We note that although thermal annealing is effective and dark current can be substantially lowered, it never regains its original pristine characteristics[19].

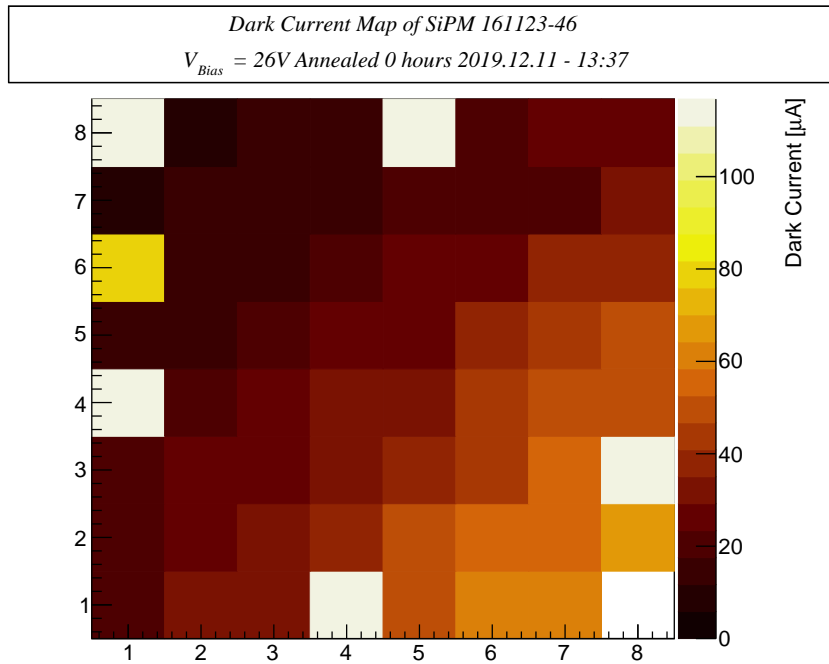


Figure 4.9: Dark current SiPM by SiPM in the array in matrix map form. SiPM 8 was pointing towards the radiation beam which is the lower right corner (see Figure: 4.6(b)), hence we observe greater dark current indicating more irradiation. Typically, dark current for healthy SiPM array is $5.1 \mu A$ with an average per SiPM dark current of $0.08 \mu A$ (see Figure: 4.19). This is a part from the report of SiPM 161123-46. Full report is attached in Appendix: A.1.

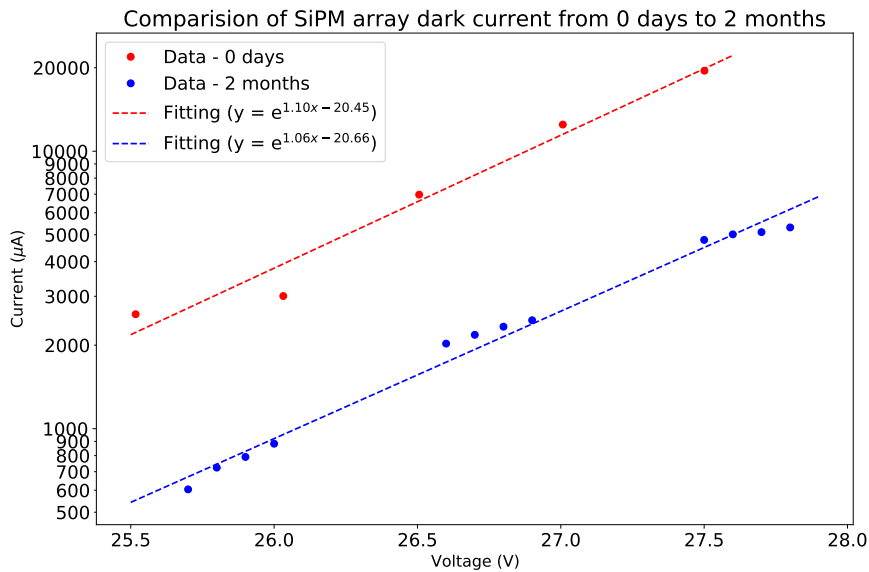


Figure 4.10: Red: Dark current data just after irradiation up to 11 Gy. Blue: Dark current data after 2 months of room-temperature self annealing.

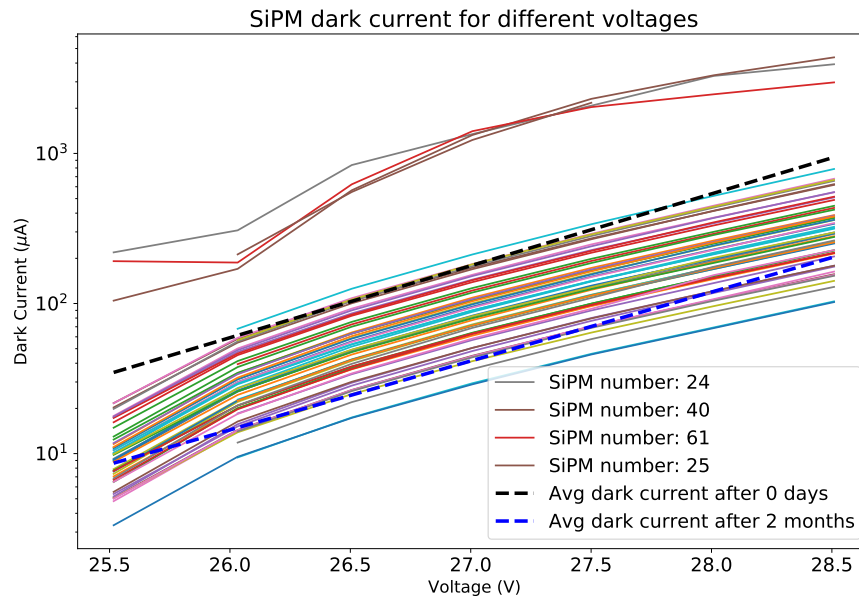


Figure 4.11: Dark current from each SiPM in the array on log scale with average dark current from 0 days to 2 months.

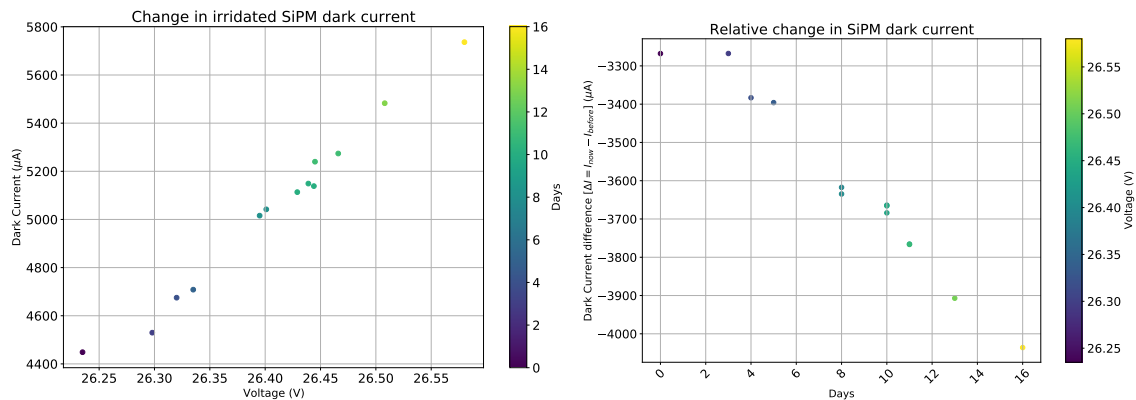


Figure 4.12: Left: Dark current readings for 16 days accounting the voltage drift. Right: Change in the dark current from 0 days to 2 months. The more negative the value, the more is the reduction in dark current.

4.4 Automatized dark current characterization of the SiPM

To characterize the SiPM array, dark current is one of the important factor, which provides information about the noise of the device (false positive triggers) and the resolution of the readings. This requires repeated measurements and altering the voltages to be able to interpret the data, usually in graphical forms. The goal of this section is to automatize this process such that it wouldn't require any human intervention and also to get a well formatted detailed report of the SiPM in question. After testing multiple SiPM arrays and comparing the generated reports, it is possible to choose the best array for the detector.

4.4.1 Design

Our goal was to be able to do the dark current measurement for the whole SiPM array and also for each SiPM in the array. We had SensL Evaluation Board (BOB3) where each

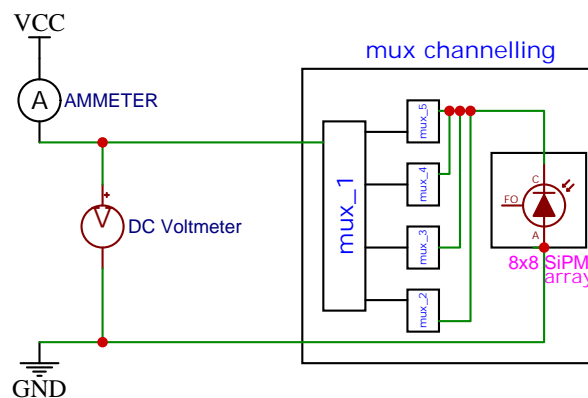
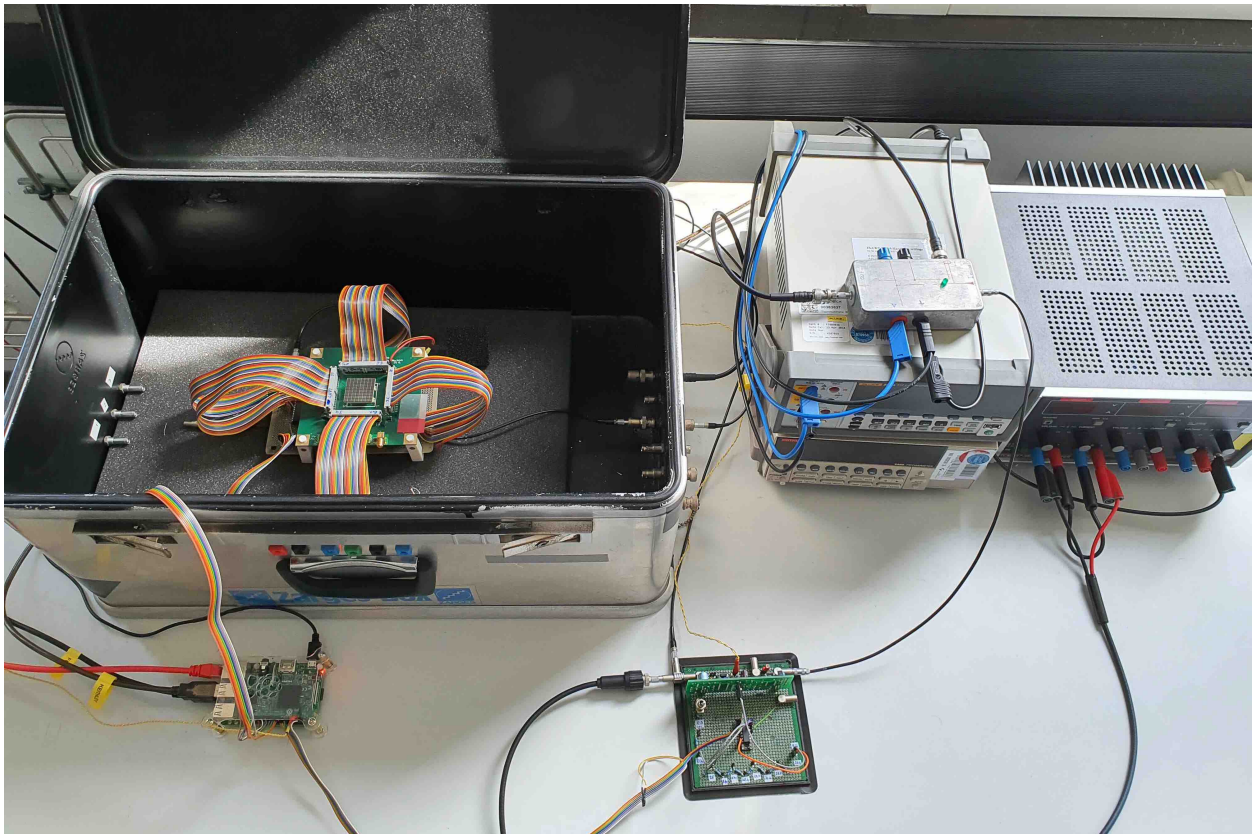


Figure 4.14: The setup of the instrument is shown in the top panel, with SiPM array with its multiplexer channelling in an aluminium box painted black inside with instruments connected. A simplified circuit schematics is shown in the bottom panel

jumper wires and the potentiometer was replaced by a set of constant resistors. Additionally, remote on/off switching was also configured using an optocoupler. In simpler terms, we can say that the potentiometer was replaced by a remote-controlled digital potentiometer which was controlled by Raspberry Pi (see Section: 4.4.1.2).

4.4.1.2 Voltage regulator

Our first approach was to add a manual rotating switch which would set a predefined resistance on the external board. A firm holder for this switch was 3D printed and assembled as shown in Figure: 4.16. During switching, there is a voltage drop to the IC (UA723) which results in very high output voltage. This required us to short the link with a much higher resistance value.

The predefined resistance was carefully calculated for the voltages we would require

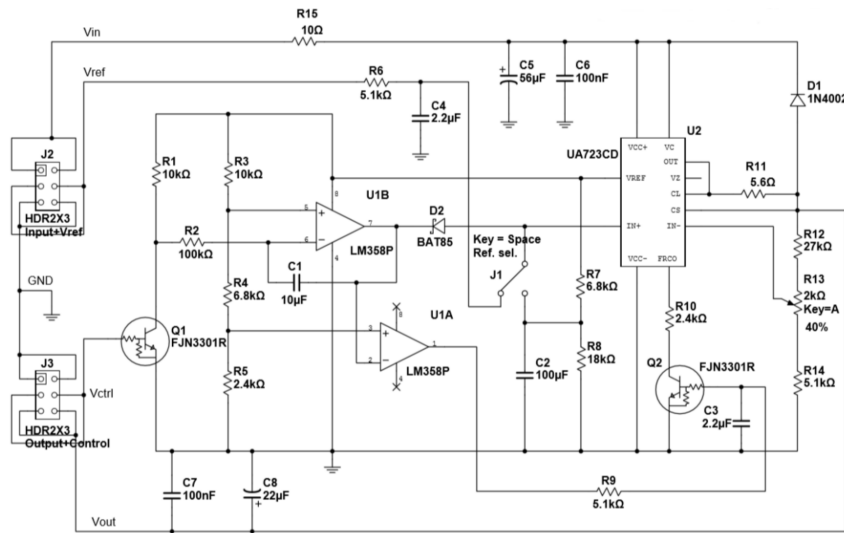


Figure 4.15: The schematics of a single module of the power supply [18]

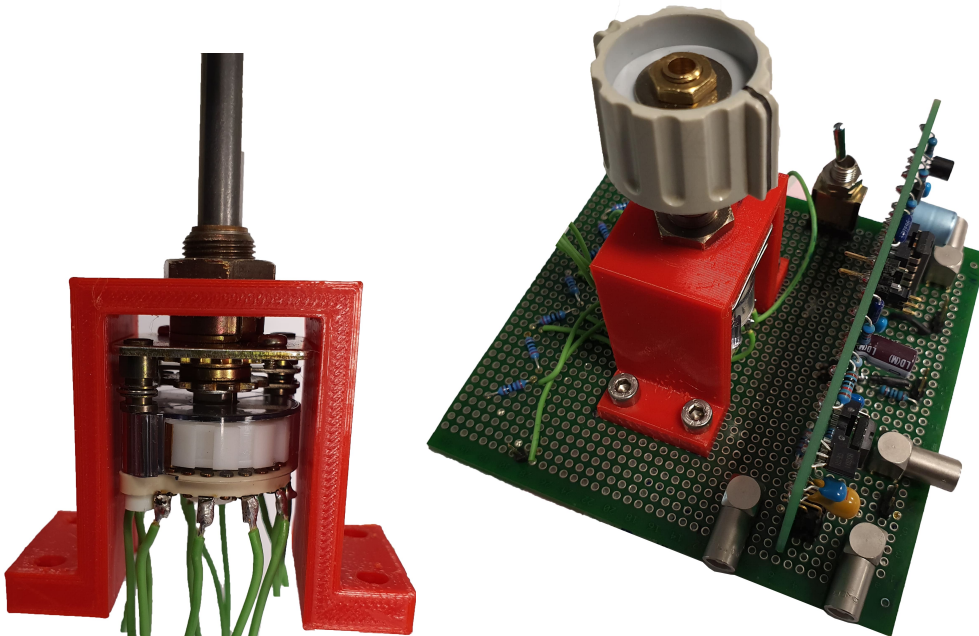


Figure 4.16: Left: Rotating switch with 3D printed holder. Right: Power supply circuit with external resistors and switch to change resistance.

for our measurements and was chosen to be a linear combination of $270\ \Omega$ resistors. The calculation for $270\ \Omega$ and $240\ \Omega$ with theoretical output voltage is tabulated in Table: 4.2. Though the change in the final voltage output is $\sim 1\ \text{V}$ for $240\ \Omega$ and $>1\ \text{V}$ for $270\ \Omega$, $270\ \Omega$ resistor was used because it has the closest value to the voltage used in the LYSO Module which is $27.0\ \text{V}$. Eight $270\ \Omega$ resistors were soldered in series and each junction was connected to the switch which bypasses the others in series, hence reducing the resistance which would in-turn change the final output voltage.

During the testing phase, it was found that this switch added an extra variable resistance ranging from $50\ \Omega$ to $250\ \Omega$ to the total resistance, and also had mechanical contact issues. This method was unfortunately discarded due to these shortcomings and the circuit was modified to make it automatic with the help of a multiplexer IC. An IC socket with a multiplexer was added to replace the switch. This was controlled by Raspberry Pi, as shown in the Figure: 4.17. The multiplexer did a similar job as the switch by selecting the total

Resistance: 270 Ω		Resistance: 240 Ω	
No. of Resistors	Theoretical voltage	No. of Resistors	Theoretical voltage
1	34.53	1	34.53
2	32.72	2	32.91
3	31.09	3	31.43
4	29.61	4	30.09
5	28.26	5	28.85
6	27.04	6	27.71
7	25.91	7	26.65
8	24.88	8	25.68
		9	24.77

Table 4.2: Calculated voltage output for the Voltage regulator

resistance, without any bulky devices or manual intervention. The IN pin from UA723 was channeled to the resistors junction making it a digital potentiometer, as opposed to bypassing/shorting resistors in series as was the case for the rotating switch. This multiplexer added a constant extra 100 Ω to the whole resistance in parallel which resulted in voltage output from 25 V with precisely 1 V increments till 32 V.

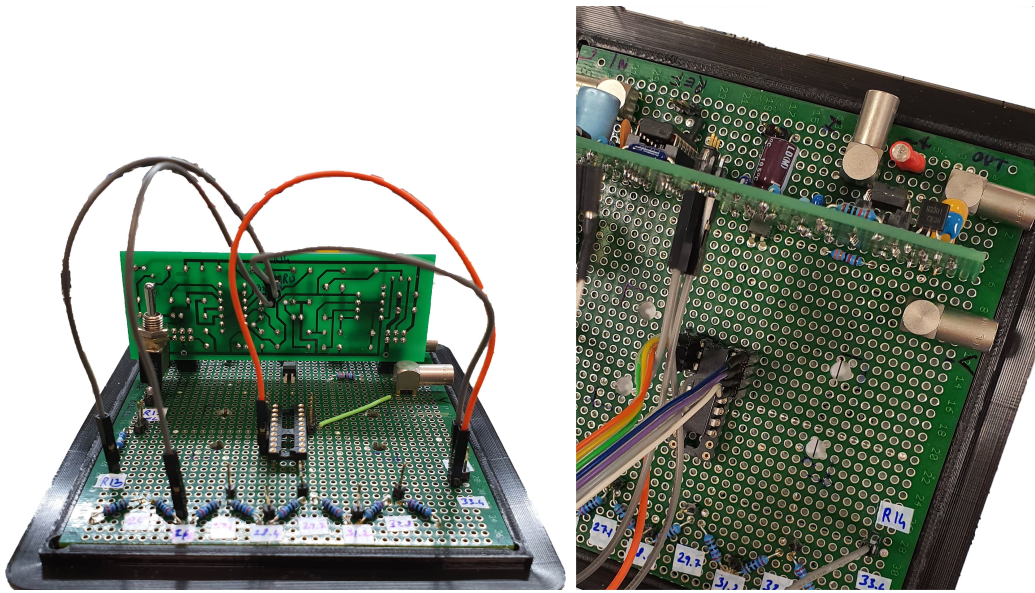


Figure 4.17: Left: Replacement of rotating switch with a IC socket. Right: Final circuit with multiplexer and connection to Raspberry Pi

At this stage Raspberry Pi was able to control the supply voltage to pre-determined voltages and also switch the power supply on/off. This allowed us to take measurements for these different voltages in a single run.

4.4.1.3 Optimized readout algorithm

Measuring the dark current of each of 64 SiPMs within the 8x8 array warms up the SiPM. This can influence the dark current measurement of the neighboring SiPMs since they are extremely sensitive to temperature as discussed in Section: 3.4.1.1. To avoid this issue, a small algorithm was developed where every successive SiPM that is being read is at least four SiPM's away from the previous one. This can be visualized in the Figure: 4.18. The colour bar shows the n^{th} reading. The higher the number (darker the colour), the later the SiPM is

read. The orientation of the SiPM matrix is similar to the other reports in this thesis. The number inside indicates the order in which the SiPM's dark current is read. This allows the SiPM to have enough time to dissipate the heat generated during the measurement. Each measurement takes approximately 15 s (including the delays and averaging) which gives it enough time to come back to equilibrium temperature of the lab.

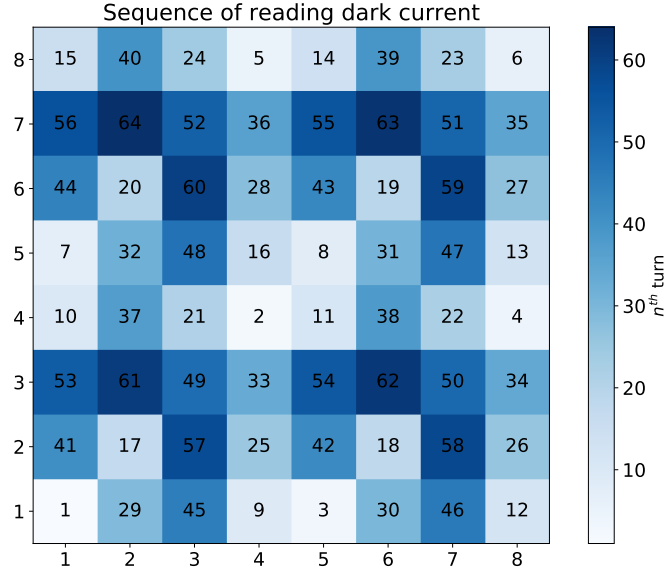


Figure 4.18: Sequence in which SiPM are read to avoid heating issue which causes an increase in the dark current.

4.4.2 Measurements

The measurement software and the post measurement analysis scripts were written with Python 3 and pyROOT package respectively, in order to take advantage of the ROOT framework by CERN[20]. The time consumption for the measurement and analysis for one SiPM array was approximately 20 minutes with the default settings, which was later modified with optimized delays and sequences to achieve the same in 15 minutes.

The measurements begin with recording of the following values:

- SiPM Serial number / Identification
- Irradiated or not?
- Annealed or not? (Only if it was irradiated)
- The duration for which it was annealed (Only if it was annealed)
- Number of averaging for pico-ammeter (Default: 5)
- Number of averaging for voltmeter (Default: 2)

After recording the input values, the software runs to take all the measurements. These are then saved as CSV files. After a measurement set is complete, an analysis script reads the recorded data and generates a detailed report.

4.4.3 Report generation with comparison

The report generation script compiles all the data and produces three kinds of reports.

- A report as single page PDF for the SiPM, for all kinds; healthy, irradiated and annealed, and with its dark current map as matrix, dark current for each SiPM and a concise table with total dark current, average, RMS, minimum and maximum dark current within the array. An example of the report of a healthy SiPM is provided in Figure: 4.19. More on this is discussed in Section: 4.3.1
- A single page report of the comparison of two annealed SiPMs where the reduction in the dark current is also calculated and shown in the report. An example of this comparison is shown in the Figure: 4.20. It also has an option for selecting any two files for comparison. The default option compares non-annealed data with all the annealed data, and last two annealed sessions. More on this report and annealing is discussed in Section 4.2

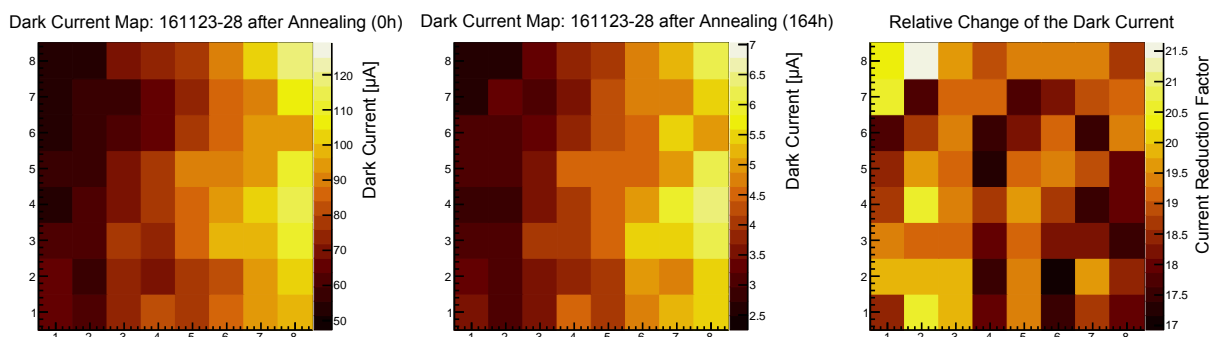


Figure 4.20: Example for the comparison report of an annealed (for 163 hours) SiPM 161123-28 with it's non-annealed data and the relative change in dark current

- (Optional) Generates a multi-page PDF with all the reports of the selected or all SiPMs and all the comparisons of the same. This is useful in-case a print is required of all the collected data or a concise PDF with all the information. The example has been omitted here since it would be a long PDF with the same information shown in Figures: 4.19 and 4.20.

Several of these reports are attached in Appendix: A.1 in the order of their serial number for reference.

4.4.4 Faults

After few runs, it was found that this set-up had an issue. There were a few random jumps in the current reading. To isolate the defective component in the set-up, first, SiPM was replaced with 27 kΩ resistor which provided comparable output of the SiPM used before. The results had similar variations, indicating that SiPM was not faulty.

After several attempts to isolate the issue by replacing each part, the only part left where the issue still occurred was the multiplexers channeling from the SensL Evaluation Board. Since evaluation board is just a separate channel connection from the SiPM, it is believed that it might be with the set-up with multiplexers, with no concluding evidence.

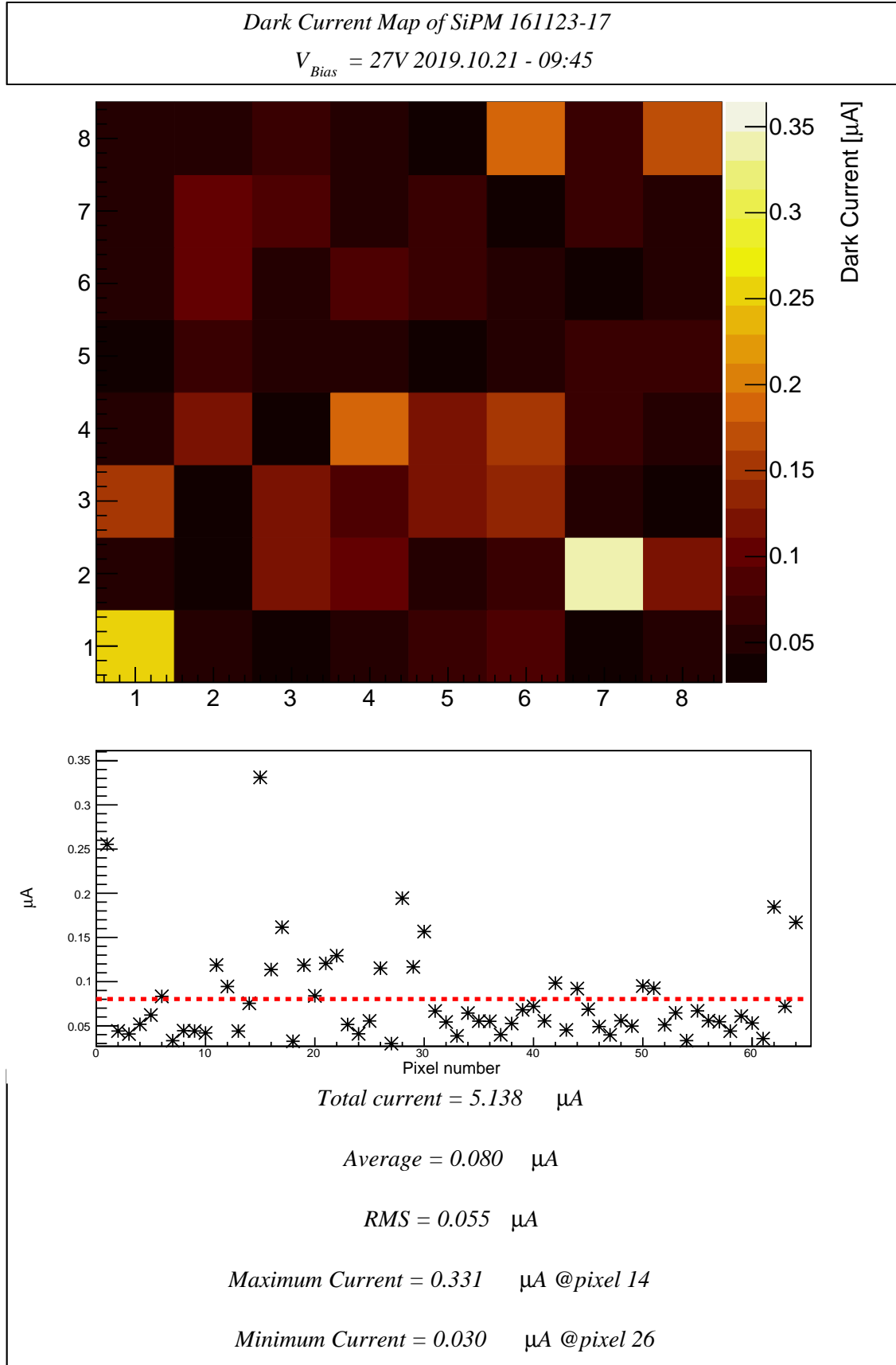


Figure 4.19: Example for the report of a healthy SiPM 161123-17

Chapter 5

Characterization of SiPM Arrays

In the previous chapters we focused predominantly on the dark current measurements of the SiPMs. In this chapter we will discuss the characterization of the SiPM by measuring the relative photon detection efficiency (PDE) and responsivity of the SiPM. Photon detection efficiency (PDE) and responsivity were previously discussed in the Section: 3.4.1.2. Since we had an array of 8x8 SiPMs, which would need individual characterization, we decided on building a mountable SiPM base with its own special illumination module. The illumination module could illuminate individual SiPMs, i.e. only one SiPM in the array at a time, where the signal from the SiPM array is recorded and this process is repeated for all 64 SiPMs in the array and the data is then processed to obtain the characterization reports.

5.1 Design

Achieving the idea of the illumination of each SiPM individually required the utilization of additional mechanical parts. The important factors that were considered while designing the instrument are as follows:

- The ability to move the illumination module in the x-y plane
- The option to control the distance of the module from the surface of the SiPM
- The angle of the xy-plane with respect to SiPM array surface

The mechanics involved the usage of two stepper motors for the navigation and planar control screws. The stepper motors and the required assembly were scavenged from the Optical Disk Drive (ODD) shown in Figure: 5.1(a). The ODD laser assembly and other unnecessary parts were stripped and the motor connections were soldered with long wires to the stepper motor drivers. Switch was added to one of the ends and 3D printed custom holder was attached to the motor shaft as shown in Figure: 5.1(b). The point where the holder, which is attached to the motor, barely touches the switch is the default starting position which will henceforth be referred as homing.

Two of such stepper motor set were assembled, one for the x-axis movement and another for the y-axis movement. It was attached to two 3D printed slates which serves the purpose of holding these assemblies.

5.1.1 Configuration of the instrument

Several combinations of the assembly were possible, for example, having both axis movements for the illumination module or for the SiPM holder alone, or one axis for illumination module

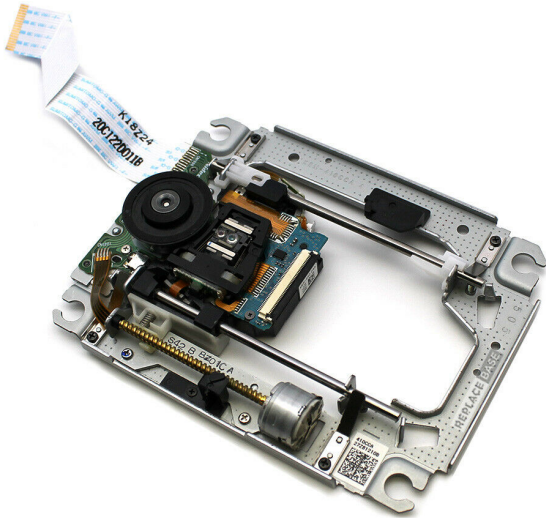


Figure 5.1(a):

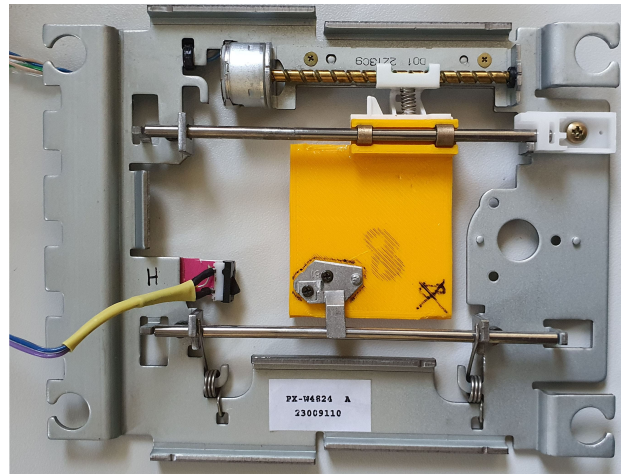


Figure 5.1(b):

Figure 5.1: Modified optical disk drive with custom 3D printed plate attached to the holder

and another for SiPM holder. Two of such combinations and their shortcomings are discussed in this section.

5.1.1.1 Coupled axis

Our first approach was to have only one moving part with other remained stationary. The illuminating module was chosen to be the moving part which could move in x-y plane while the SiPM holder was fixed at a place. All the necessary parts and attachments were 3D printed and the assembled CAD object of the slates is shown in Figure: 5.2(a). The set-up was such that the illumination module was on the top, as shown in Figure: 5.2(b) with a pen laser attached as illumination module for demonstration purposes.

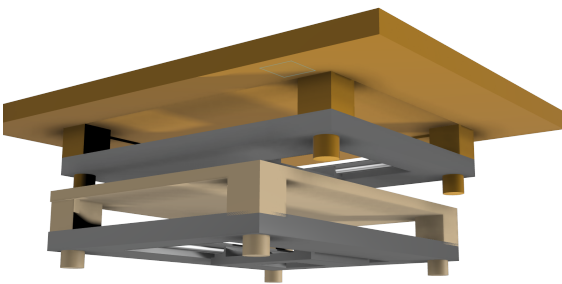


Figure 5.2(a):

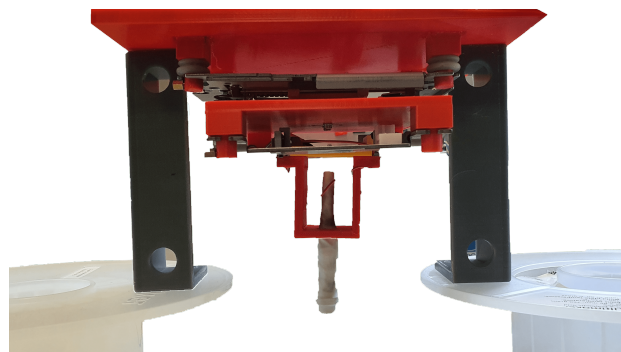


Figure 5.2(b):

Figure 5.2: (a) CAD object assembled in Autodesk Fusion 360. (b) 3D printed structures assembled with pen laser as illumination module.

Testing: This set-up was put to test, during which we found that:

- There was a lack of overall stability

- The whole structure was heavy for the motors, because of which the motor skipped counts/steps

Because it was essential to overcome these issues, a different structure was proposed which is discussed in the next section. By replacing motors with more powerful ones with appropriate drivers, one can solve these issue in this case.

5.1.1.2 Separate axis

The new structure was made by rearranging the holding plates, where the SiPM holder moves along one axis, while the illumination module moves along an orthogonal axis, so that the overall movement of both remained confined to the xy-plane.

One of the assembly was mounted on the base slate where the SiPM holder was soldered with the LEMO connectors. The contacts of the assembly to the base slate were also fitted with a silicon cap to reduce the vibrations from the mechanical movements.

Illumination module holder was made to have a 2 cm x 2 cm socket which mounted on the slate inverted along with two 3D printed pillars supporting the top slate. These pillars were attached on the base slate, in a way such that the illumination module outlet points to the corner SiPM in the SiPM array in the default configuration where both the assemblies rest after homing. The final set-up of the instrument is shown in Figure: 5.3. Due to the stricter lockdown for controlling the COVID-19 pandemic, implemented on a very short notice before the holidays, travelling to the lab for an picture was not possible.

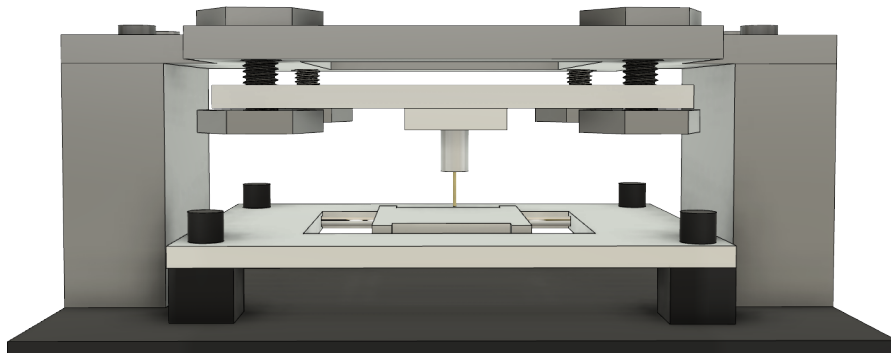


Figure 5.3: CAD object assembled in Autodesk Fusion 360 with the illumination module.

5.1.2 Characterization of LED and reference SiPM

In order to use the LED and reference SiPM in the illumination module in Section: 5.1.4, we need to understand their characteristics. The following subsections discuss the characterization along with the setup and circuit for each of these components. In the basic setup the LED was connected to the signal generator and SiPM was connected to the oscilloscope through the readout circuit. A power supply unit was connected to the SiPM for providing the reverse bias potential.

5.1.2.1 Photon spread of the LED

A red LED was chosen to be used in the illumination module, and therefore was characterized. The LED was mounted on the board with current limiting resistor of $50\ \Omega$ and LEMO cable

was used to connect the LED to the source. Tektronix AFG3252 signal generator was used as the source voltage for the LED. To remove the reflecting signal due to the usage of the coaxial cable, a terminal $50\ \Omega$ resistor was added in parallel. This is shown in the Figure: 5.4. A 2x2 SensL C-series ($6\times 6\text{mm}^2$ with $60\ \mu\text{m}$ pixel size) SiPM was used as the photo-detector, and was placed 8 cm from the LED as shown in Figure: 5.5. We made sure that both were equally elevated from the base by a measure of 35 mm.

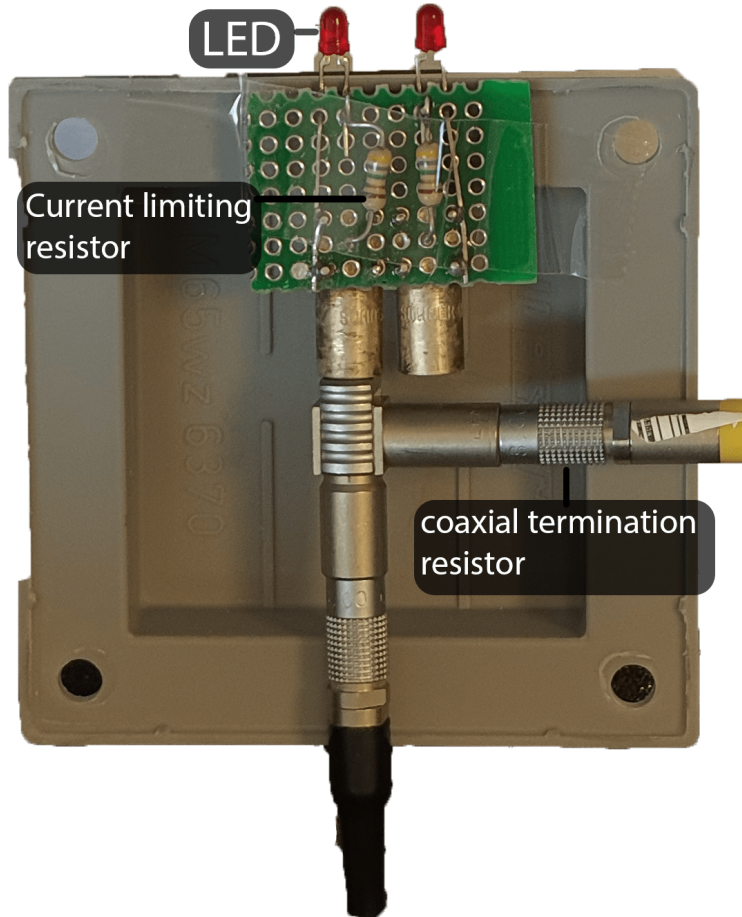


Figure 5.4: LED setup used for characterization with $50\ \Omega$ current limiting resistor at 5 V and $50\ \Omega$ coaxial termination resistor

The signal generator was set to 1-cycle, burst mode with 1 kHz repetition rate. A square shaped pulse signal was set with a supply voltage of 2.5 V. The width of the signal specifies the time duration for which the voltage is being supplied. The set-up was placed inside a box painted black from inside. The signal from the SiPM was recorded for different widths of the signal to the LED with every 10° angle change on both clockwise and anti-clockwise up to 40° .

Figure: 5.6 shows the peak SiPM signal for different signal widths of the LED from -40° to $+40^\circ$ angles. One can see that the spread of the light at all widths has the same structure with respect to the angle, since the distribution of the photons remains the same. The amplitude of the SiPM signal increases with increasing the width, as expected, because the number of photons produced increases. Also as expected, the amplitude is at its highest at 0° and decreases gradually as the angle increases, finally drops to very low values after 40° . For angles up to $\pm 10^\circ$ the light distribution appears to be sufficiently spread indicating that within this range it can be considered to be the same.

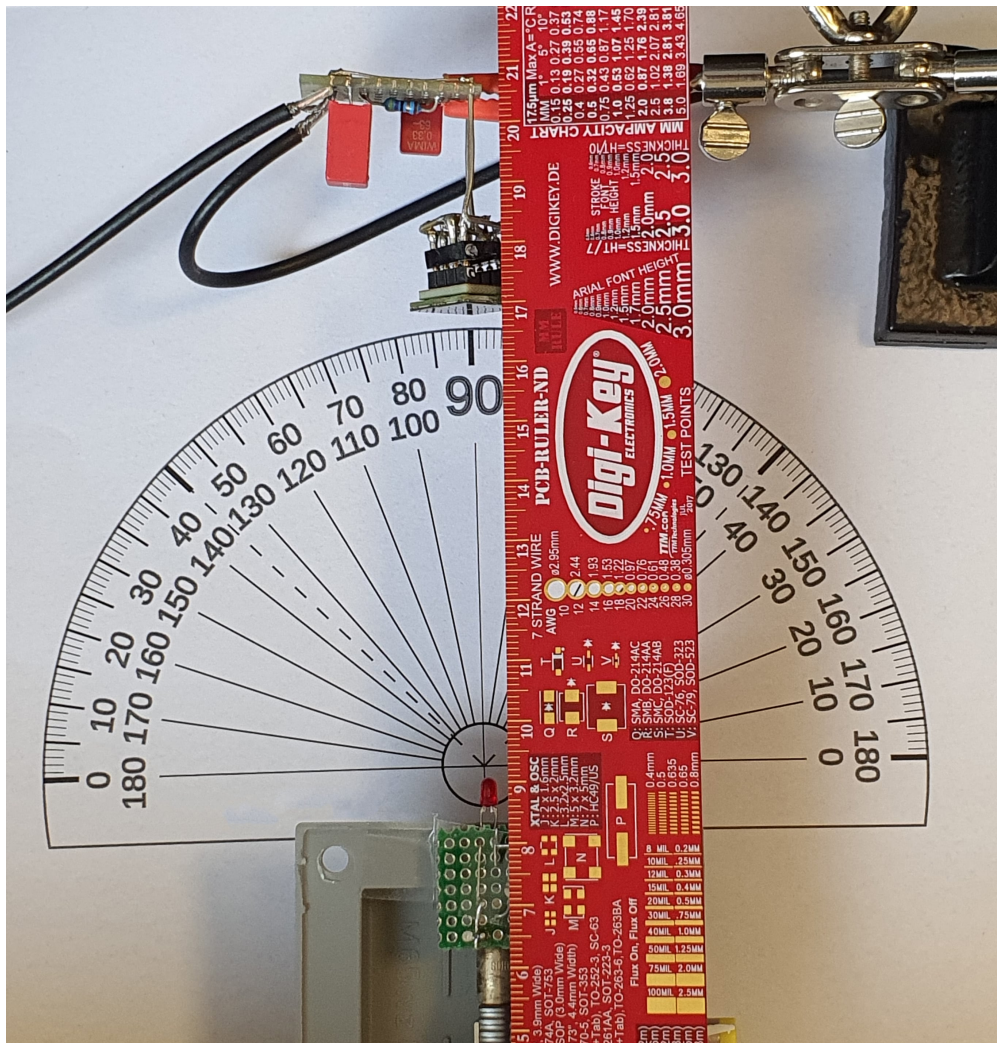


Figure 5.5: Set-up for LED photon spread at different angles

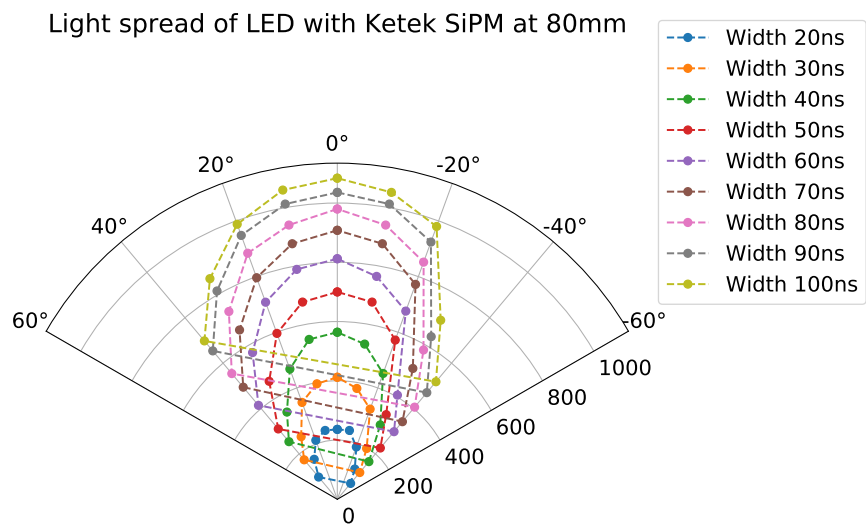


Figure 5.6: LED photon spread for different increasing interval of supply voltage. Angles are in degrees and radii are in mV

5.1.2.2 Saturation of Reference SiPM

Reference SiPM array, used in the above section - SensL C-series, was set-up with an SiPM readout circuit with supply voltage filter as shown in Figure: 5.7.

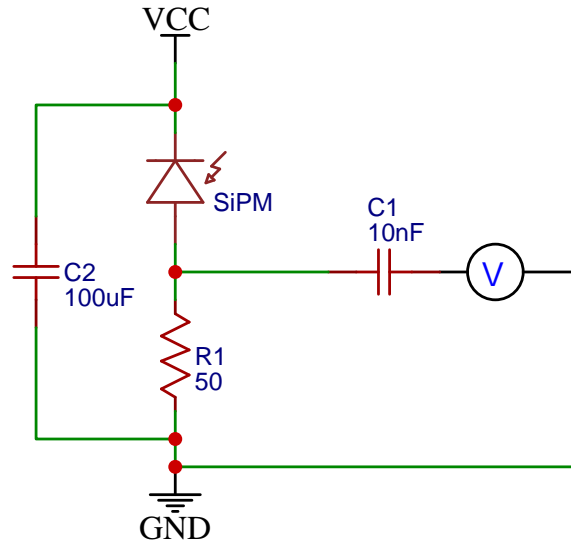


Figure 5.7: Circuit schematics for readout of reference SiPM

The SiPM was reverse biased at 30 V. The LED was inside a module and was 1 cm apart from the SiPM. A prototype version of the actual illumination module is discussed in the next section. Voltage from the generator was set to 2.5 V. The signal from the SiPM was probed with an oscilloscope.

From Figure: 5.6, we observe a decreasing spacing between the curves at a particular angle, as the widths are increased. Therefore, the voltage measurements were made as a function of the width for two filters; one consisting only one white paper and the other with two white papers. The corresponding result is shown in in Figure: 5.8.

Curves corresponding to both the filters reach a plateau, attaining different values for the maximum voltages. Since upon increasing the thickness of filter, the maximum voltage decreases, it can be inferred that the SiPM is not saturated in this case. The addition of the filters allow for the recovery of more microcells before the other microcells are triggered.

In case of saturation, both the curves should result in the same maximum voltage. In other words, all microcells are fired almost simultaneously. A short burst of very bright light can trigger all the microcells almost simultaneously, leading to a saturation.

An important point to note from Figure: 5.8 is that very long flash of light would not provide any useful information. Furthermore, it does not mimic the scintillating light flashes where the maximum width of the light would be around 100 ns (with decay time 40 ns for the LYSO scintillating crystal, light at 80 ns is approximately 8 times smaller). During this experiment, we could also understand that flashes of light, which are shorter than 80 ns, are more useful and do not let the voltage saturate. Hence, the maximum width of the signal to the LED was limited to 100 ns. For the course of this thesis, 40 ns was used as default width hereafter unless otherwise mentioned.

5.1.3 Angular absorbance of SiPM array

To determine the effects of the angle of incidence of the incoming photons, a small set-up was made. The SiPM array was fixed at a place, while the LED (red colour) pointing towards

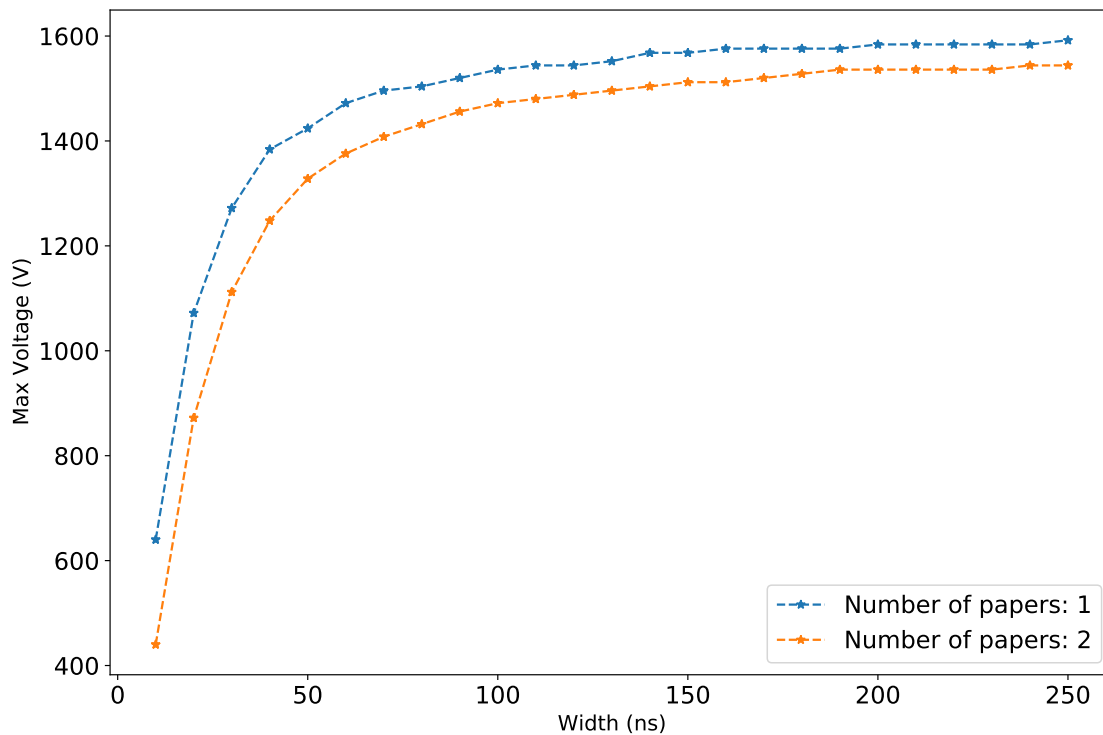


Figure 5.8: SiPM voltage as a function of width for SiPM reverse biased at 30 V and LED voltage at 2.5 V

the center of the SiPM array was moved on the circumference of radius 8 cm. The LED was biased at 5 V with width of 100 ns. The signal peak from the SiPM array was recorded for every 10° degree angle. Figure: 5.9 shows the angular absorbance of the SiPM array, namely 161123-03. One can see an increase in the voltage peak for -10° degree which is due to the reflection from the adjacent LED (the characteristic of the setup, see Figure: 5.4).

Apart from this deviation, the absorbance seems similar up to 30° , indicating that the incident photon angle can vary in small values without having any significant differences in the measurement values. While the top illumination module holder (see Section: 5.1.1.2) has the option to change the xy plane, small human error while setting this plane parallel to the SiPM arrays plane will not contribute significantly to the existing instrumentation error.

5.1.4 Illumination module

The idea of this instrument was to illuminate each of the SiPM and to measure the signal. SiPMs are extremely sensitive to photons and in order to characterize several of them, it requires the conditions to be exactly the same for each SiPM in the array during the measurement. Therefore a few important points considered during the design were:

- The area of illumination should be limited to that of the SiPM
- The photons should have maximum diffusion or distribution
- Measuring the output light or a reference signal to normalize the data

The ideal goal was to have the ability to change or modify the illumination module as needed. Hence this module was made completely independent from the rest of the instrument and it is used as an additional attachment. This will be inserted into illumination module holder which has a 2 cm x 2 cm opening.

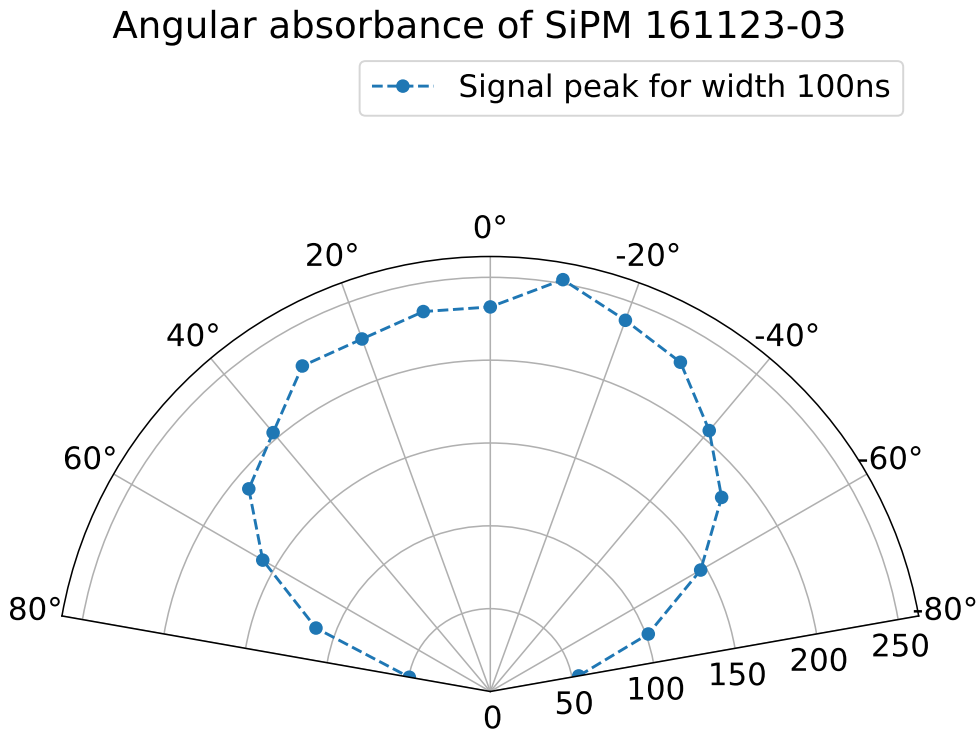


Figure 5.9: Angular absorbance of SiPM array 161123-03 at 5 V for signal width of 100 ns. Angles in degrees and radii in mV

In the design, it was made to fit in the 2 cm x 2 cm socket with the characterized LED and reference SiPM. The SiPM holder was placed at an angle of 45° with respect to the LED holder. There is also a provision to add filters in front of the SiPM.

The body of the module had extruded hollow cylinders for screws to support and hold the body with the cap. Two small carvings were made in the design - one for the LED wire and another for the reference SiPM. The opening hole to the SiPM was printed to be 2.8 mm x 2.8 mm to counter the diffraction at the edges. CAD model of the module along its cap is in the Figure: 5.10

Components: A reference SiPM was placed in the SiPM holder with Tedlar sandwiched between 2 white papers as a filter to avoid the saturation of the SiPM at higher widths, as discussed in Section: 5.1.2.2. A red LED in a rectangular mould was placed in the LED holder. Co-axial cables were soldered to both the components to avoid electromagnetic interference which used to produce damping oscillations in the reference SiPM signal. The wires were taken out through the 2 designated holes and the cap was screwed.

Figure: 5.11 shows the 3D printed module with all the components. The print was done in red, assuming that it has sufficient density to confine light completely since red light will be reflected due to the nature of colors. Later it was found that there was a small light leakage because of which black vinyl electrical tape was used to cover the module.

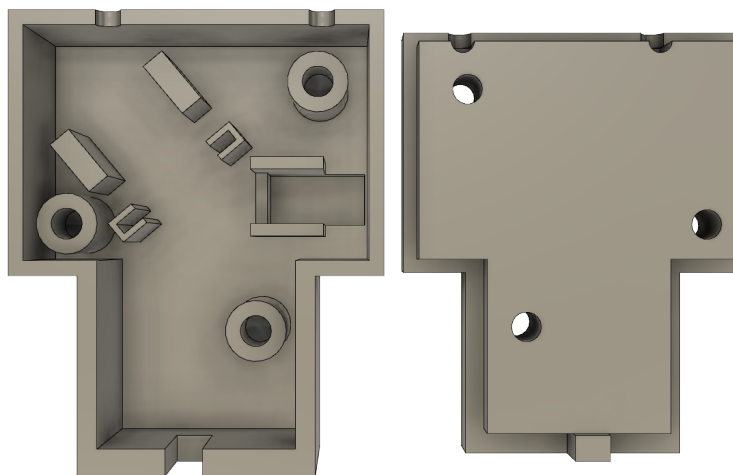


Figure 5.10: Illumination module model with its cap, 3 screw holes, reference SiPM holder, filter holder and LED holder

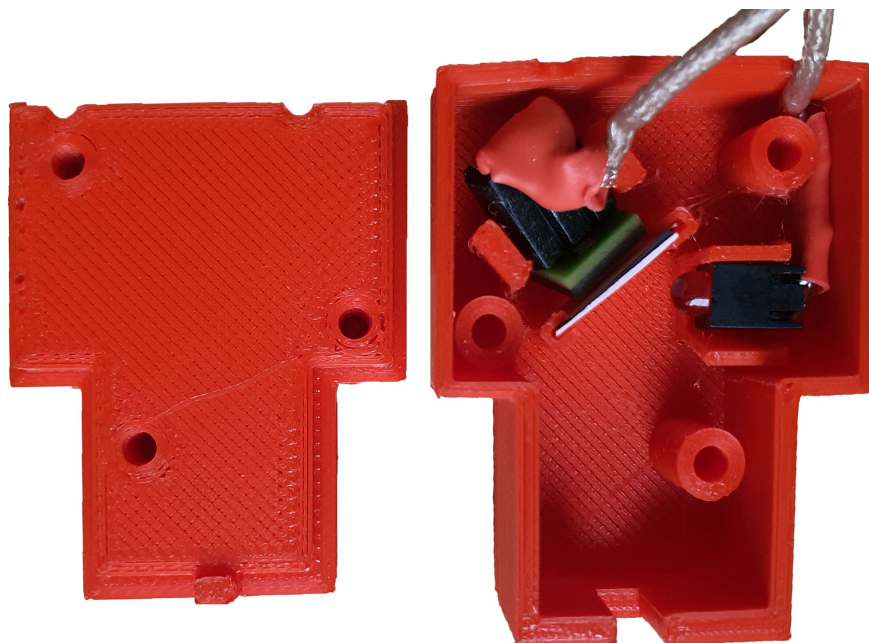


Figure 5.11: 3D printed illumination module with SiPM, filters and LED

5.2 Measurements

The setup was controlled by RedPitaya board with the GPIO controllers. GPIO pins were connected to a circuit with motor driver with 12V power supply and switch pins. Power supply for the bias voltage was drawn from a power supply unit and the signal from each SiPM was connected to different channels of the oscilloscope. The LED was connected to a function generator. The software was written in Python 3 ran on RedPitaya and can be executed by SSH or using in-built Jupyter web interface. Due to the hardware limitations, on-board analysis was not possible and a separate script had to be executed on a different computer on the network to generate the reports.

The measurement data is recorded in row-wise sequence according to the SiPM numbers in the board in a single line, row wise. Total measurement takes approximately 15 minutes including network based report generation.

5.3 Reports

The report produced for the relative charge $q_{\text{SiPM array}}/q_{\text{ref SiPM}}$ is shown in Figure: 5.12. Since the scale is relative, it is dimensionless. Values close to unity or greater, show better responsivity than the lower ones.

It was observed that in the absence of SiPM or a defective SiPM, there are reflection / scattering events which result in a small signal from the array which is less than 30% of a healthy SiPM signal. In general, relative charge values less than 0.7 can already be considered to be poorly performing while those less than 0.4 corresponding to a dead SiPM. In special circumstances, values for a poorly performing or dead SiPM can be varied with a calibration SiPM array which also includes a dead or missing SiPM in the array.

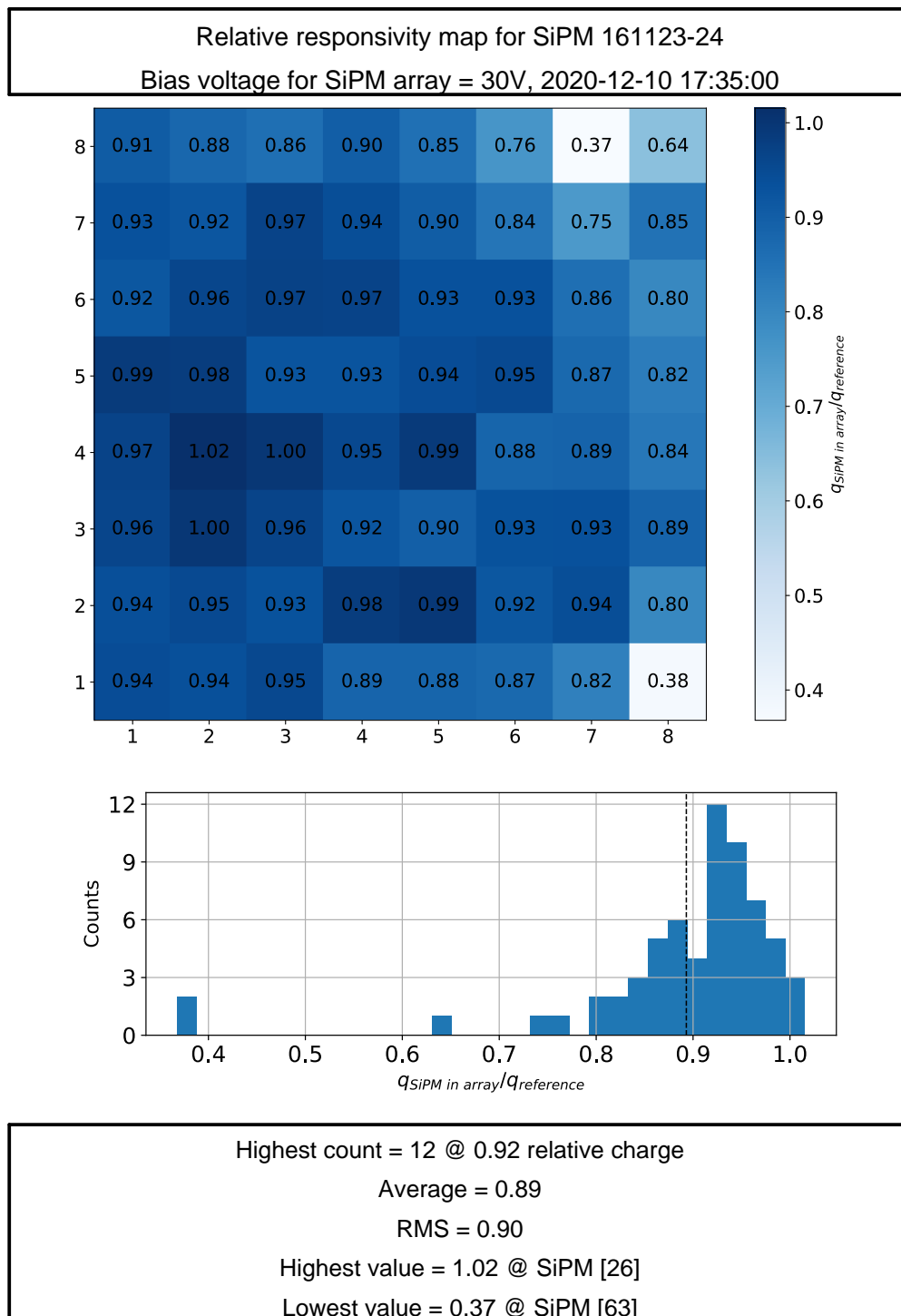


Figure 5.12: Relative charge map for the SiPM array. SiPM 8 and 63 are missing and the small readings are due to the reflections and scattering and hence this is taken as the lower bound.

Chapter 6

Summary and Outlook

The accidental irradiation of the SiPM served as a motivation to study the radiation hardness and radiation damage of the SiPM. An irradiation experiment was therefore set-up, and a test SiPM was subjected to high intensity radiation in a controlled environment. A dedicated standalone dark current measurement set-up was constructed to record the dark current readings and to analyse the data, generating a report, in order to understand the relation of the radiation dosage to the dark current. Moreover, SiPMs were subjected to annealing, both at high-temperature and room-temperature, and followed by further measurements, in order to study the effects of annealing on the SiPM. The former was observed to have much better results than the latter.

Another dedicated measurement set-up was constructed to measure the responsivity of the SiPM, where a reference SiPM was used to normalize the signal from the SiPM array. This set-up had moving mechanical parts where each SiPM was illuminated individually during the measurement. After the measurement, the data was analysed on a remote computer over network and the report for responsivity was generated.

These reports constructed a basis enabling us to sort the SiPMs according to their health, leading to choosing the SiPM in the best condition to be used in the future experiments for the JePo.

In order to further improve the measurement set-ups, one can upgrade the motor drivers to support the 1/32 stepping, so that much finer movements are possible. Additionally, an illumination module with different color LED would also be interesting to study, especially if the application of the SiPM is changed. Probably, allowing a larger base area, the set-up could also be customized to work with larger arrays. Currently, the RedPitaya is limited by hardware to analyse. This means that a better hardware would eliminate the need of network computing where the data could be analysed on-board during the measurement.

Appendix A

SiPM 161123-46 Report

SiPM 161123-46 was used in Irradiation of SiPM at Cyclotron (Section: 4.3).

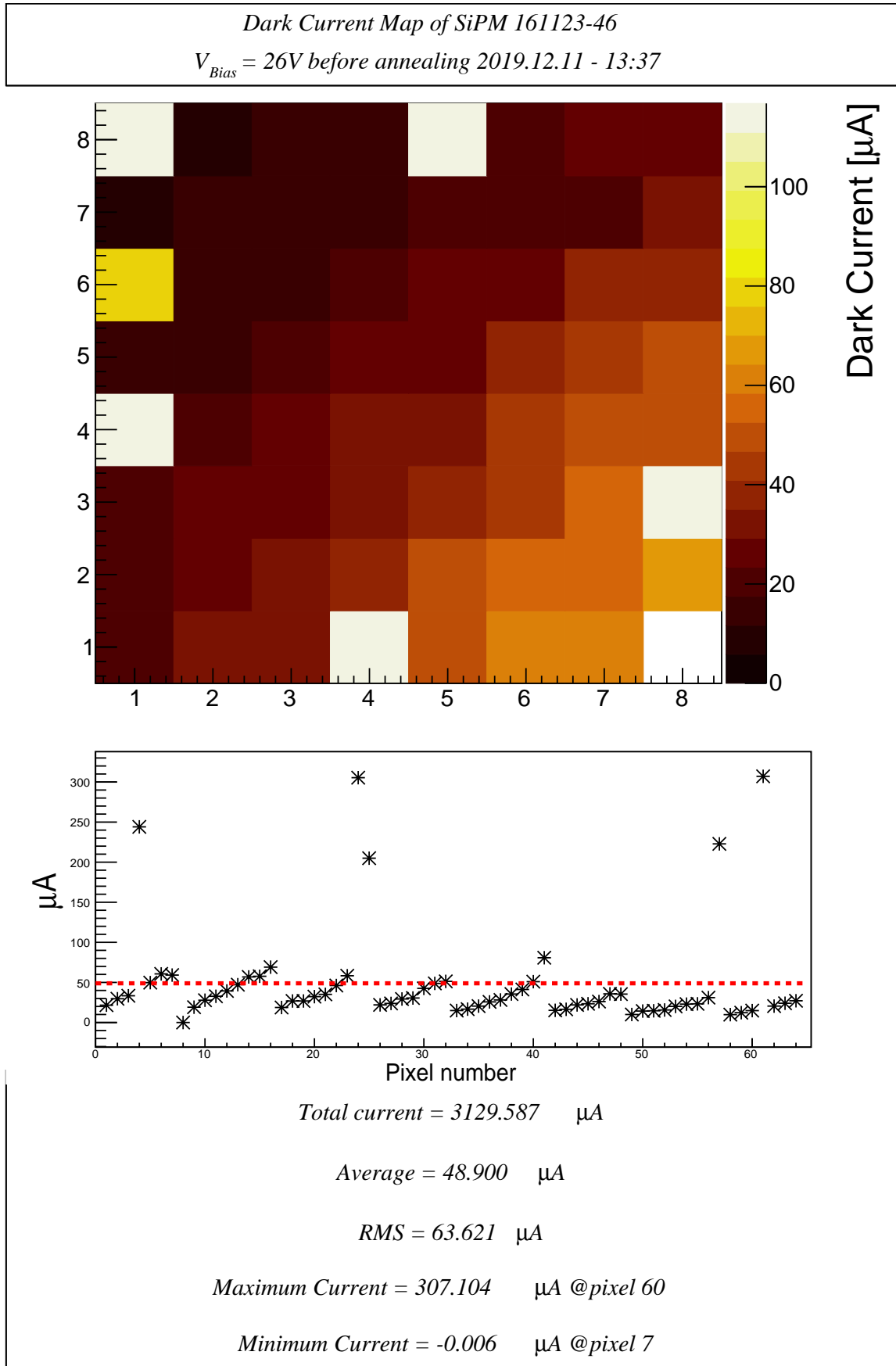


Figure A.1: The compiled report of 161123-46 SiPM used in the irradiation of SiPM in the Section: 4.3

Appendix B

SiPM 161123-07 Report

SiPM 161123-07 was one of the accidentally irradiated SiPM in COSY (Section: 4.1). It was annealed several times up to 266 h and the reports of a scan from 26 V to 30 V is attached in this chapter which created by the tool discussed in Section: 4.4. With the help of the same tool. a cross comparison of annealing at different annealed periods are attached after the individual reports.

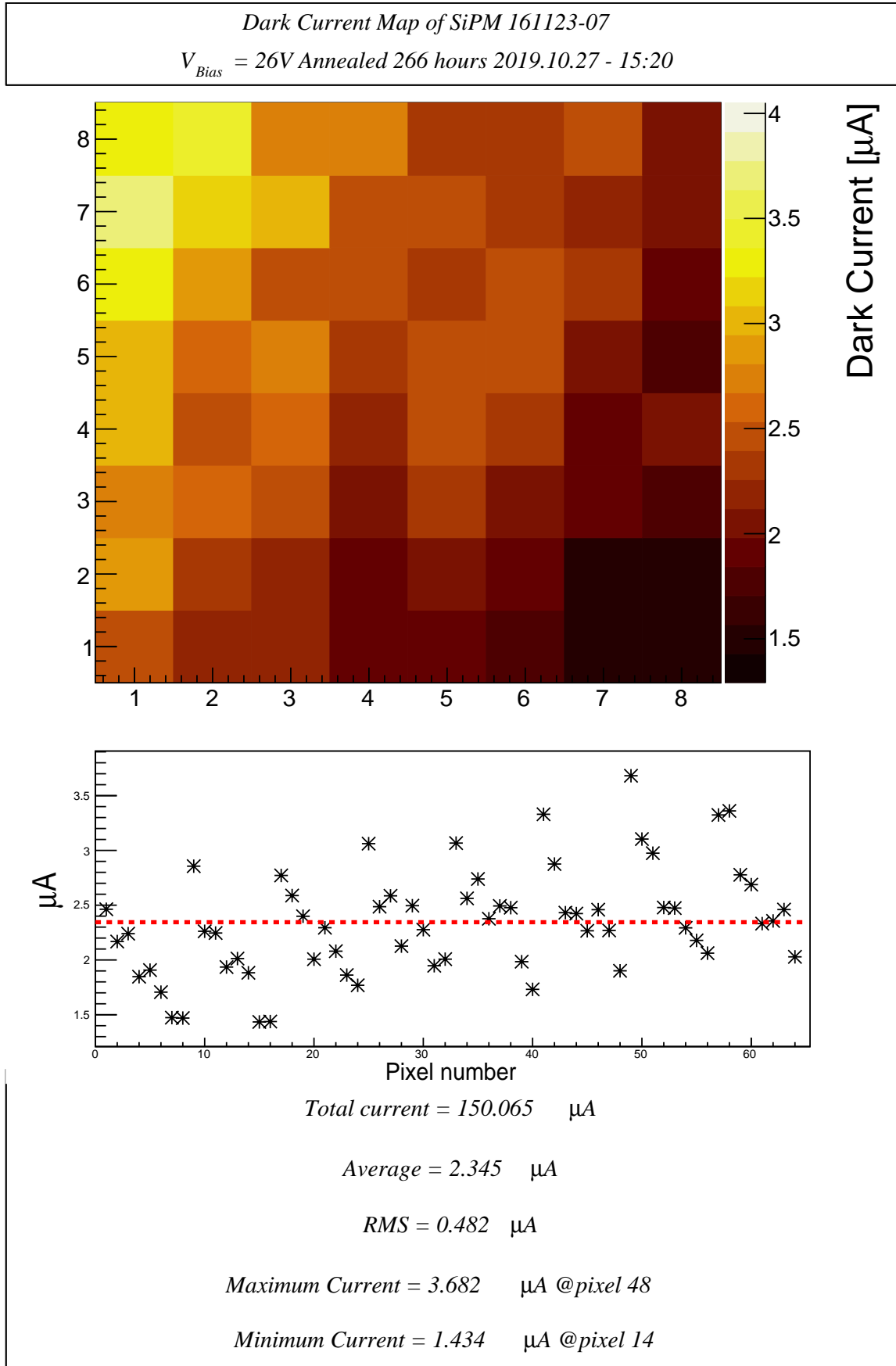


Figure B.1: Dark Current map at 26 V after 266 h of annealing

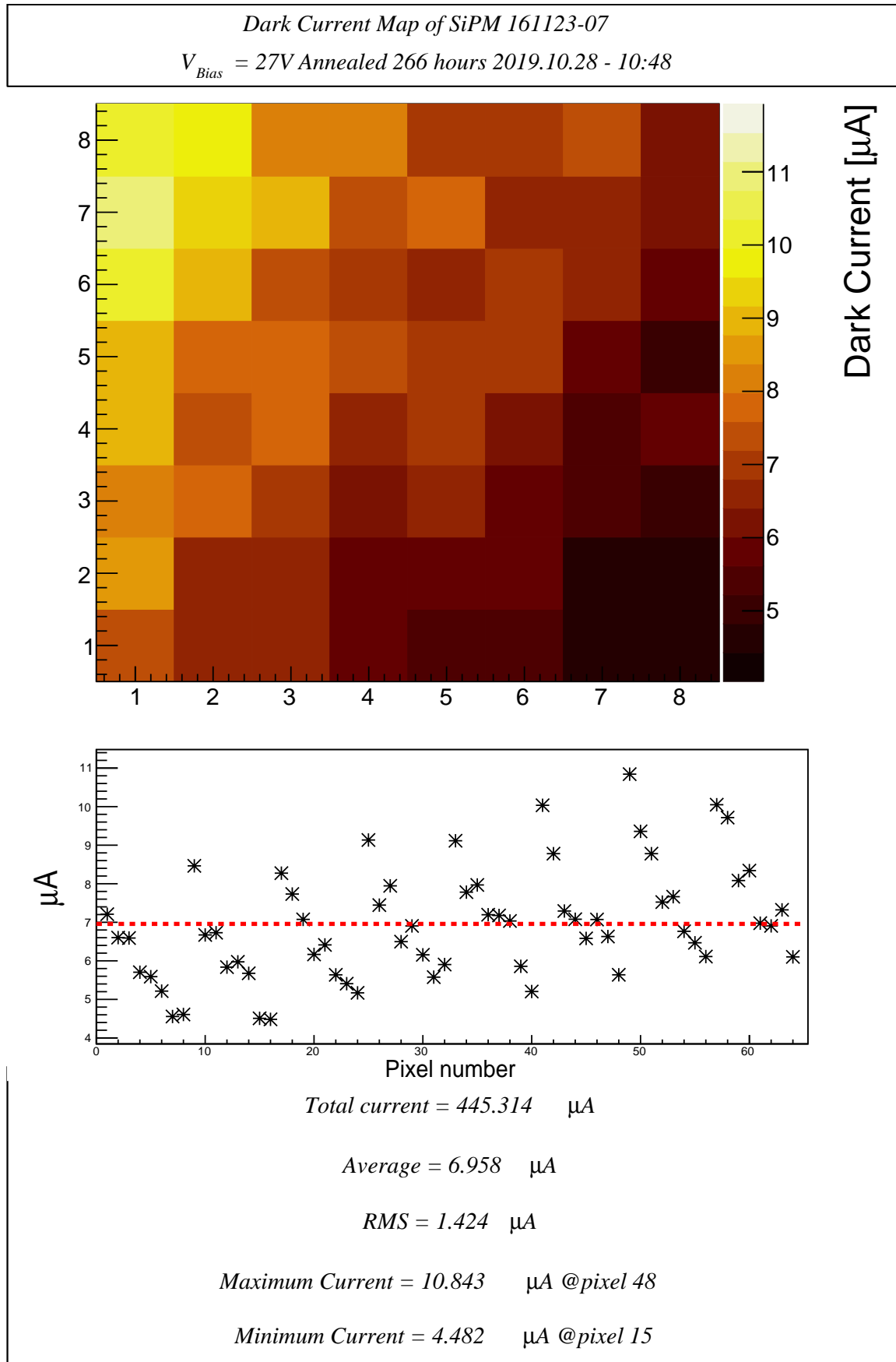


Figure B.2: Dark Current map at 27 V after 266 h of annealing

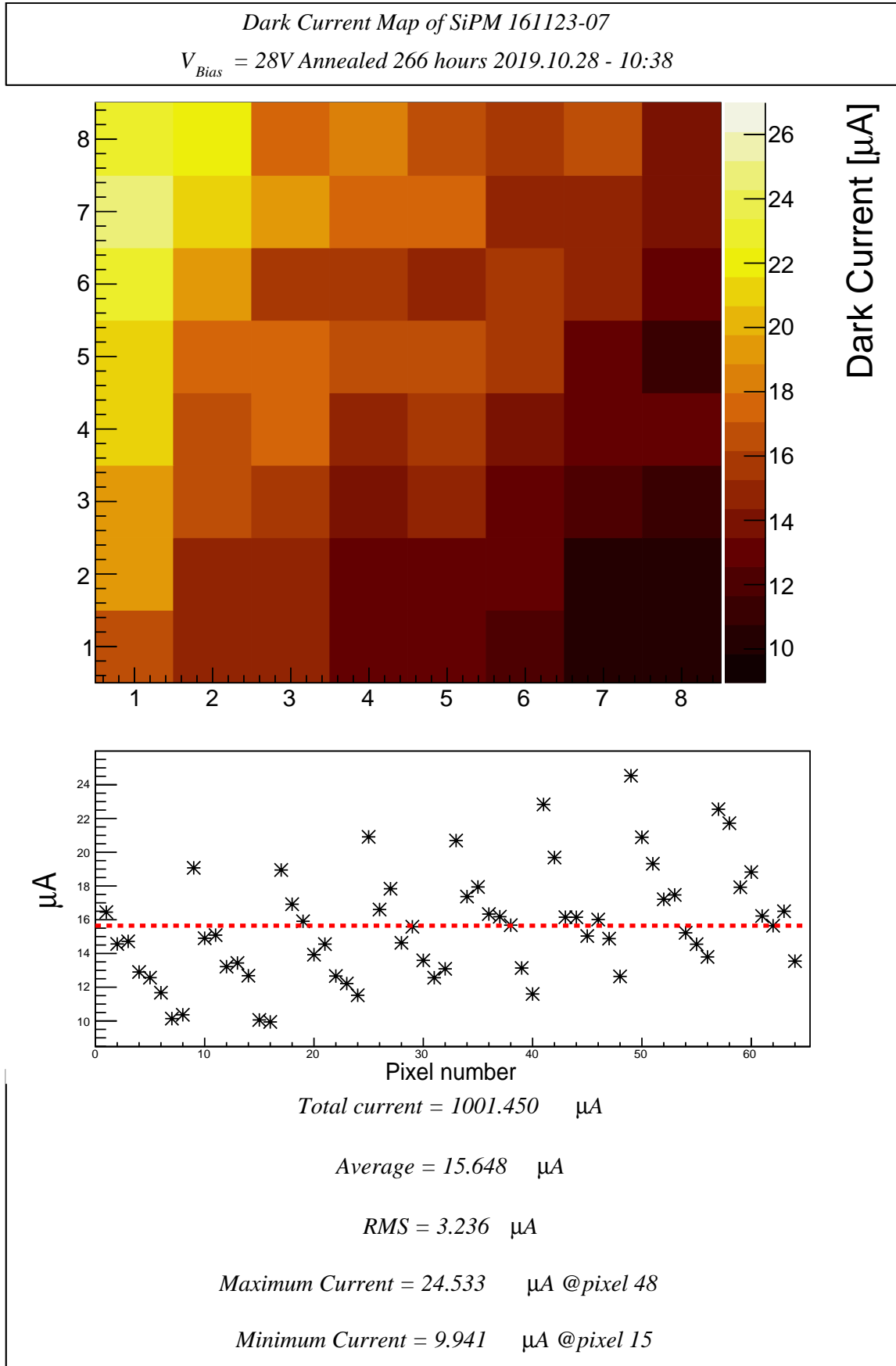


Figure B.3: Dark Current map at 28 V after 266 h of annealing

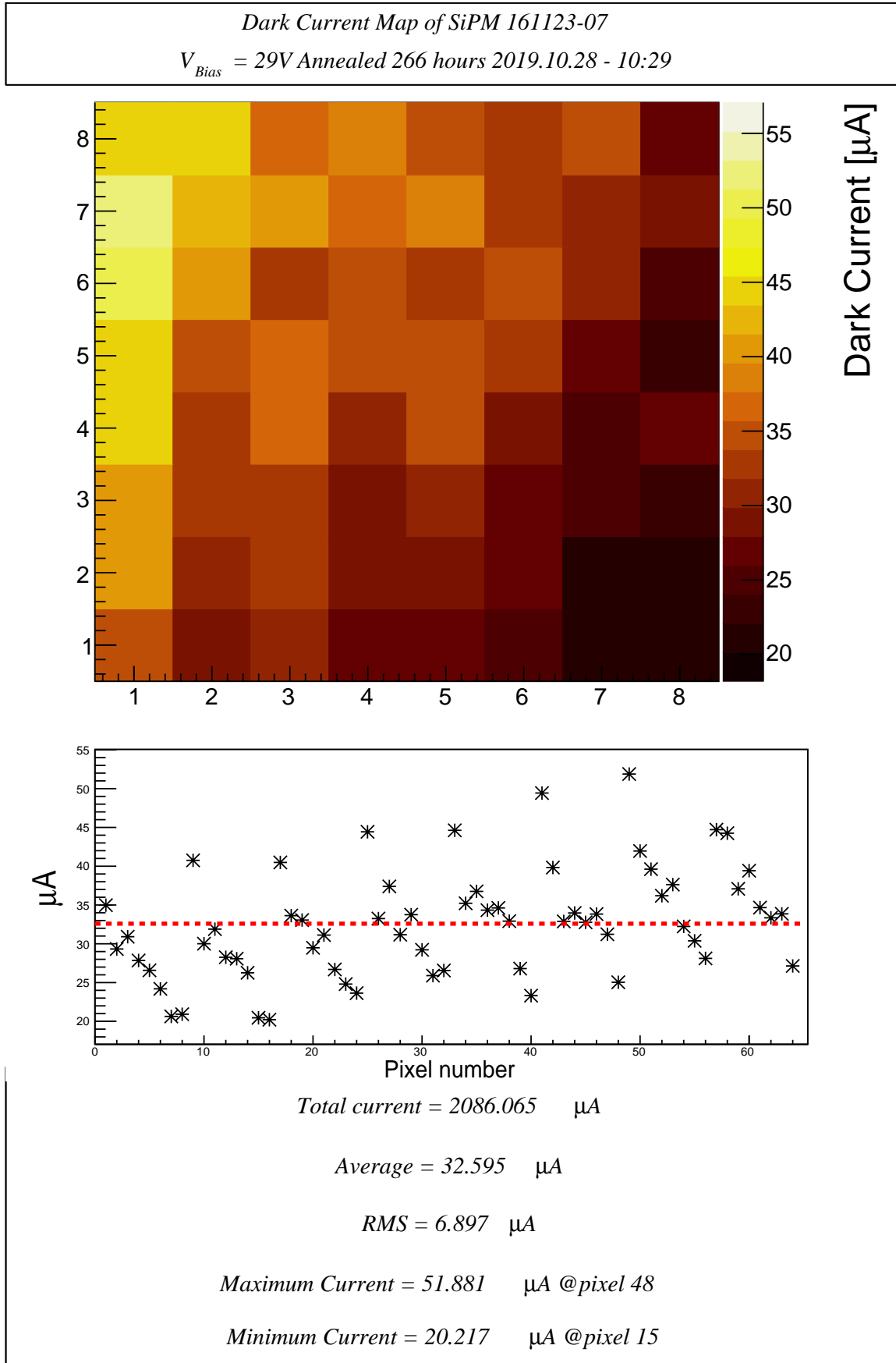


Figure B.4: Dark Current map at 29 V after 266 h of annealing

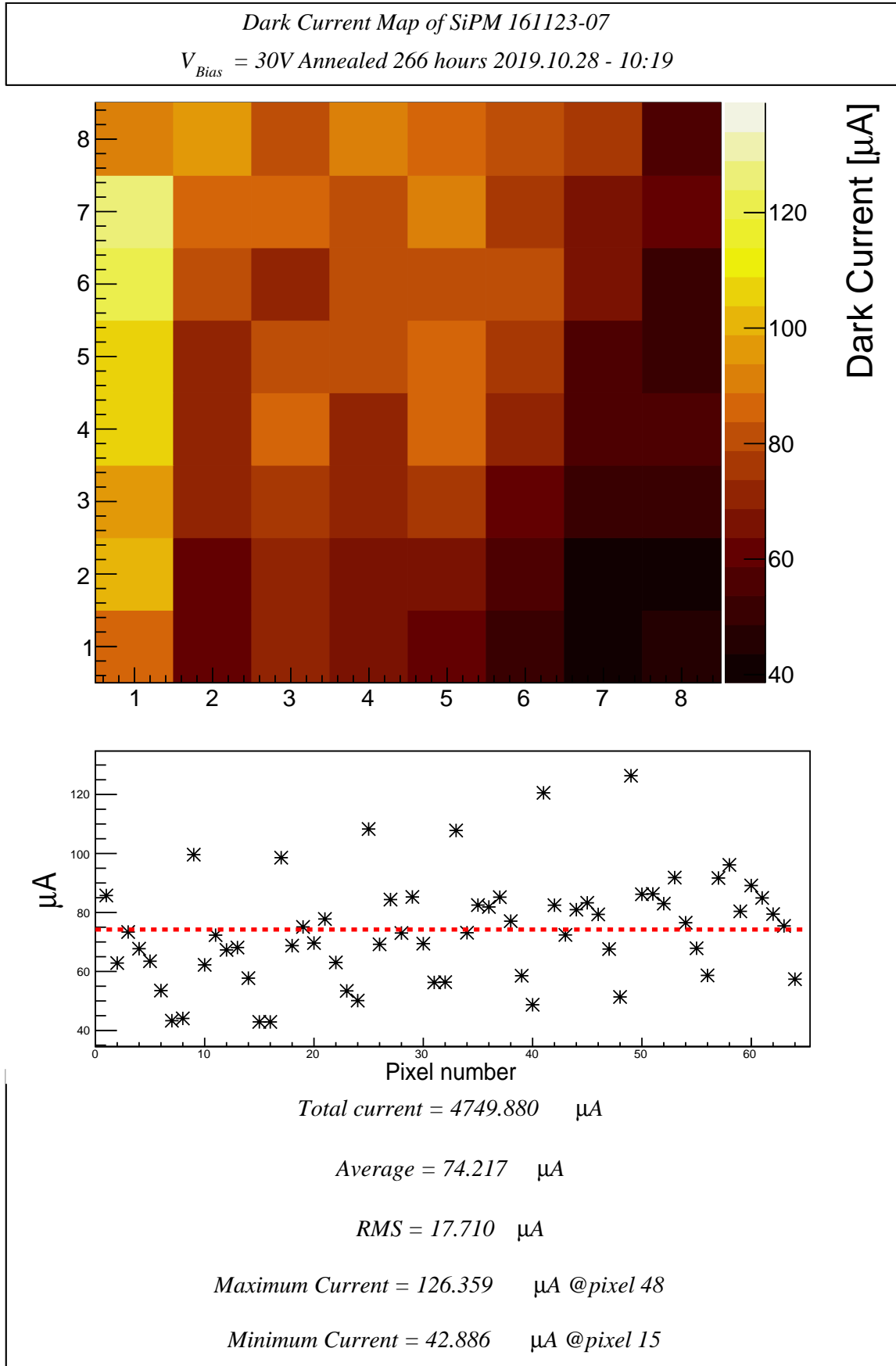


Figure B.5: Dark Current map at 30 V after 266 h of annealing

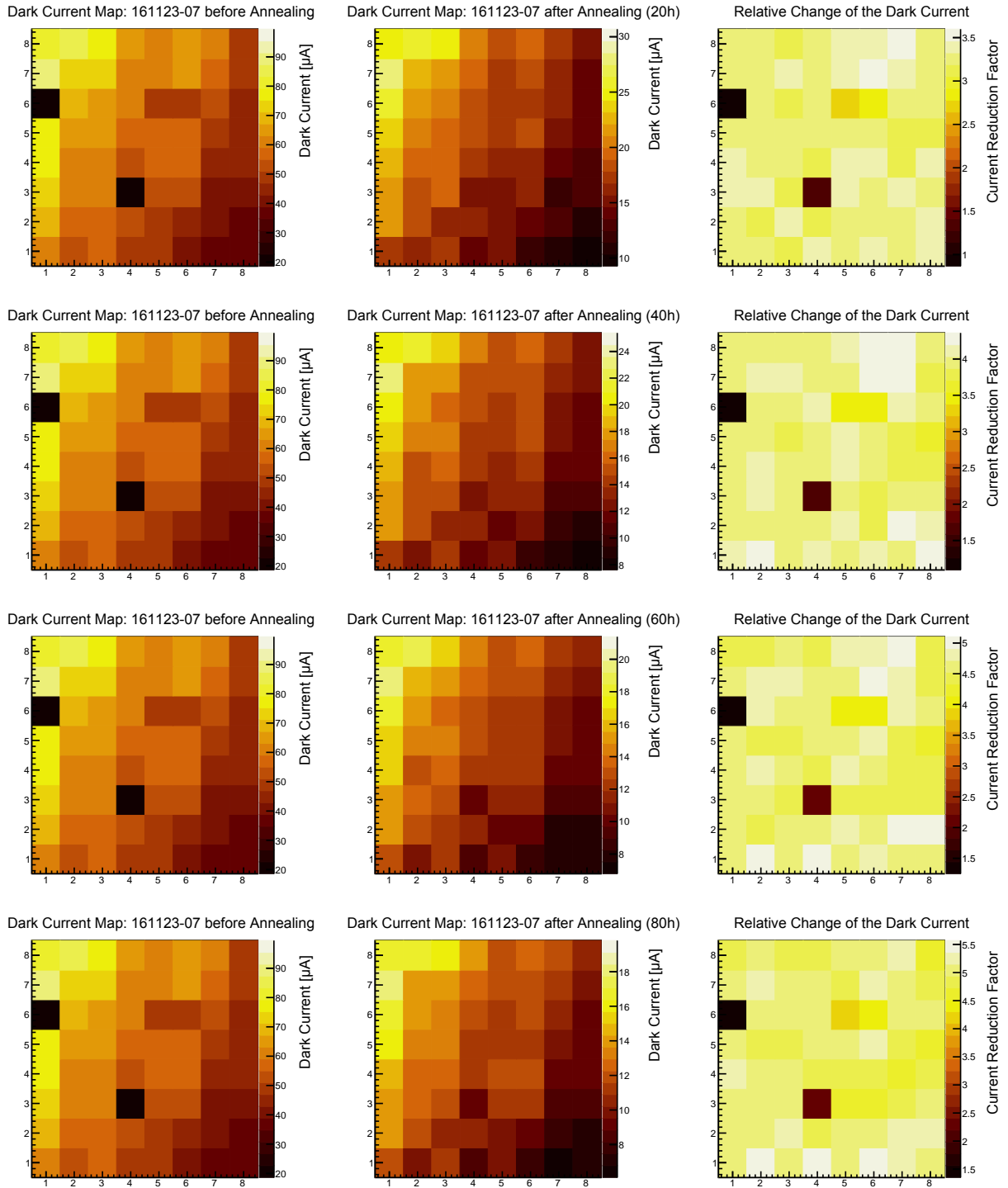


Figure B.6: Dark current comparison for each annealing session with non-annealed including the last 2 sessions

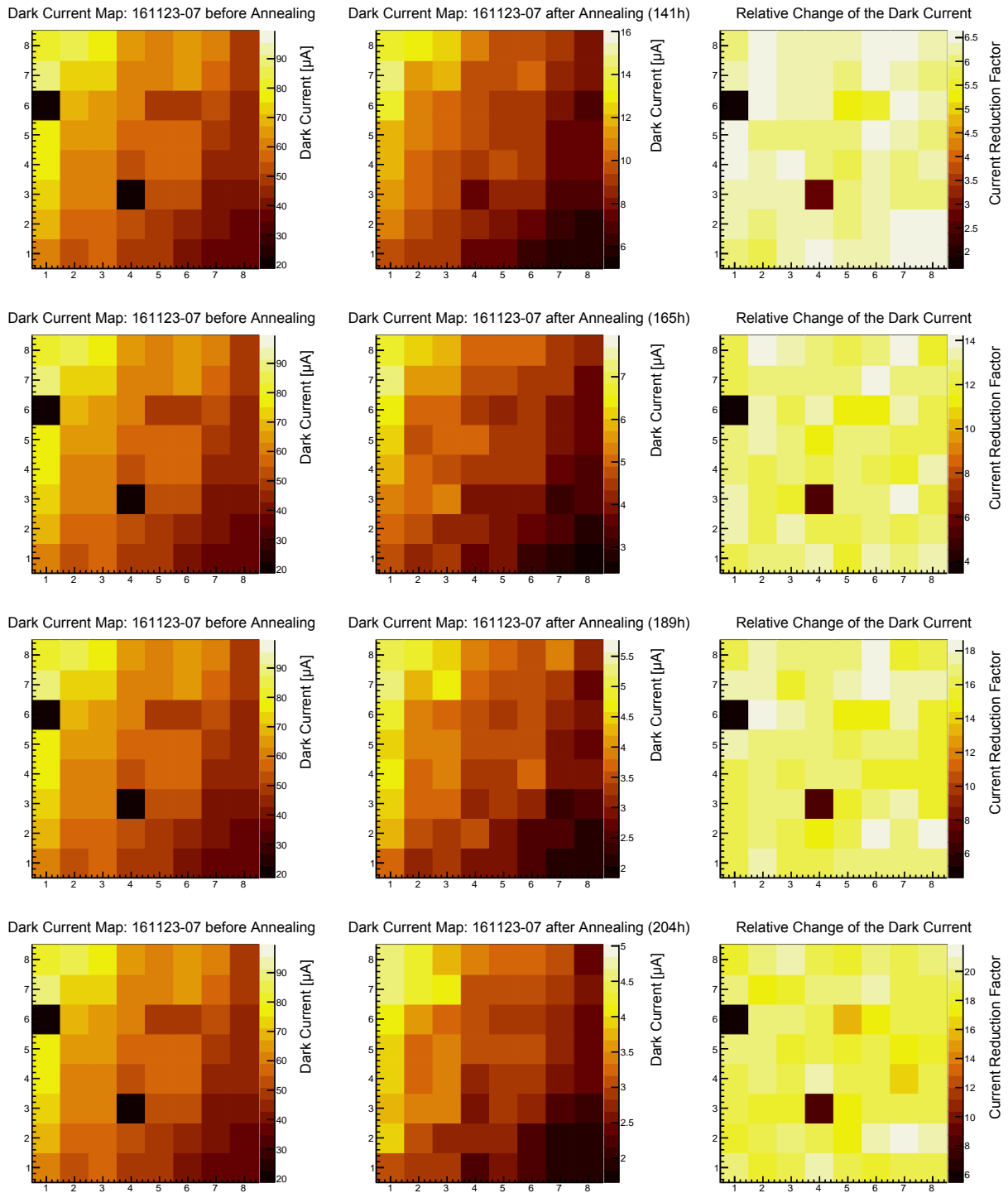


Figure B.6: Dark current comparison for each annealing session with non-annealed including the last 2 sessions

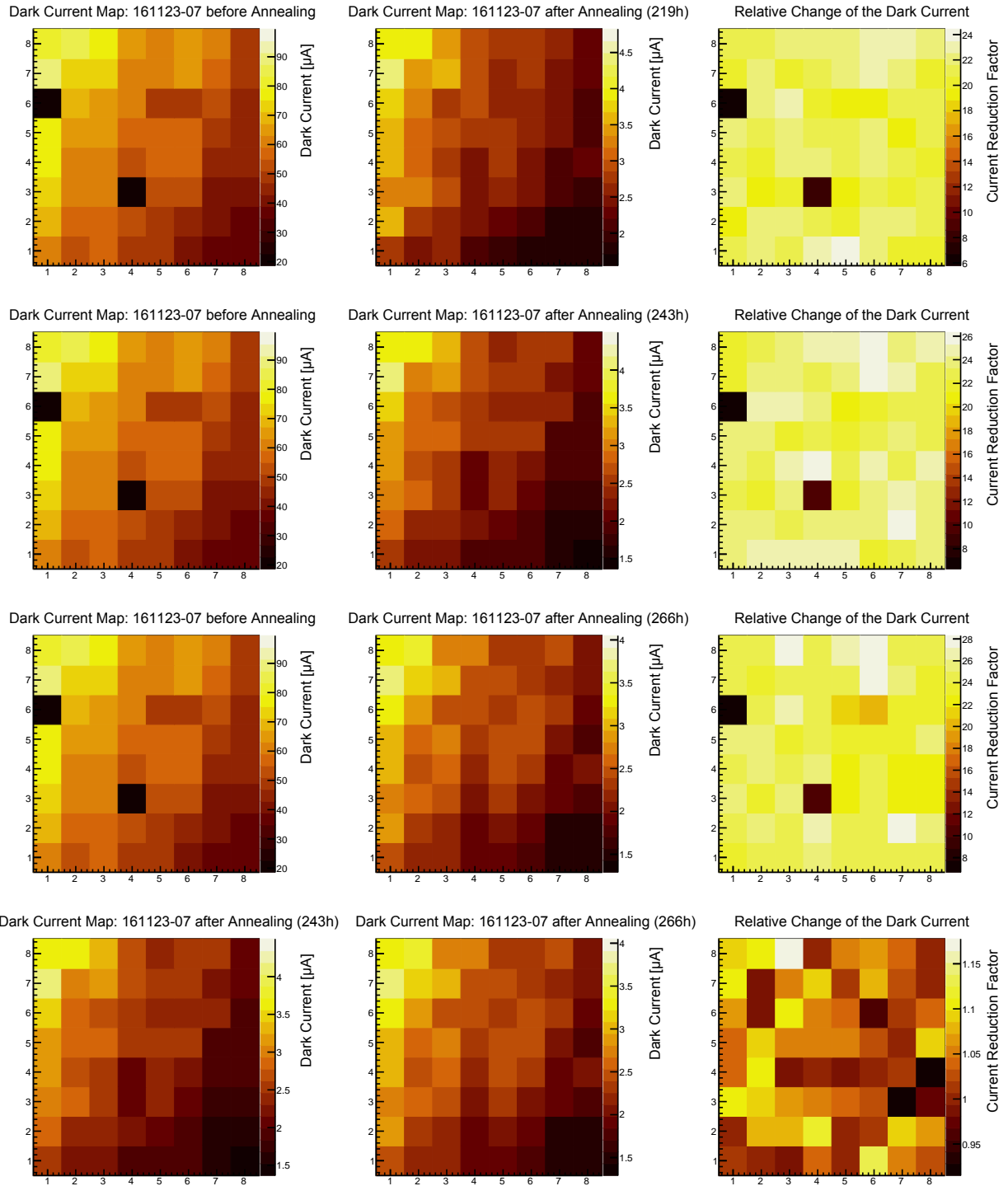


Figure B.6: Dark current comparison for each annealing session with non-annealed including the last 2 sessions

List of Figures

3.1	Cooler Synchrotron (COSY) at Forschungszentrum Jülich	10
3.2	Jülich Light Ion Cyclotron (JULIC) in Cooler Synchrotron (COSY) at Forschungszentrum Jülich	11
3.3	A unit of ΔE detector in JEDI polarimeter - LYSO crystal, SiPM array along its readout and mounting case and the holder	11
3.4	JEDI polarimeter in COSY	12
3.5	The arrangement of the ΔE detectors in JEDI polarimeter[5]	13
3.6	Temperature dependence of operating voltage and dark count rate[12]	14
4.1	Dark current readings for the SiPMs in JePo as arranged in Figure: 3.5 on October 15, 2019, after the accidental irradiation. Center marked 'x' shows the beam pipe center. For each box, SiPM channel number is on the top with it's dark current in μA	18
4.2	Comparison of dark current of thermally annealed SiPM 161123-07	19
4.3	(a) Location of the experiment - JULIC. (b) Experiment was placed at the end of the cyclotron ring.	20
4.4	(a) CAD object of the SiPM holder and the cap created in OpenSCAD. (b) CAD objects assembled into a single unit.	21
4.5	Experiment setup with Tedlar and dosimeters.	21
4.6	(a) Radiation film was placed on the experiment to understand the distribution of the radiation. (b) Small radiation film was placed on the SiPM. The lower part had greater exposure to the radiation and hence the film is darker	21
4.7	Dark current readings during the experiment when the radiation was off. Accumulative of both the days with different dosage rate.	22
4.8	Linear Regression fit to the obtained data, only for the rate 3 mGy/s.	23
4.9	Dark current SiPM by SiPM in the array in matrix map form. SiPM 8 was pointing towards the radiation beam which is the lower right corner (see Figure: 4.6(b)), hence we observe greater dark current indicating more irradiation. Typically, dark current for healthy SiPM array is $5.1 \mu A$ with an average per SiPM dark current of $0.08 \mu A$ (see Figure: 4.19). This is a part from the report of SiPM 161123-46. Full report is attached in Appendix: A.1.	24
4.10	Red: Dark current data just after irradiation up to 11 Gy. Blue: Dark current data after 2 months of room-temperature self annealing.	24
4.11	Dark current from each SiPM in the array on log scale with average dark current from 0 days to 2 months.	25
4.12	Left: Dark current readings for 16 days accounting the voltage drift. Right: Change in the dark current from 0 days to 2 months. The more negative the value, the more is the reduction in dark current.	25

4.13	Comparison of dark current readings (in JePo as as arranged in Figure: 3.5) at 27 V with UNI-T multimeter in JePo, after the accidental irradiation in October (left panel) to a later measurement in January (right panel). The center, marked as 'x', shows the beam pipe center. For each box, SiPM channel number is on the top with it's dark current in μA . Since SiPM channel 40 was repaired and exchanged, it does not follow the trend.	26
4.14	The setup of the instrument is shown in the top panel, with SiPM array with its multiplexer channelling in an aluminium box painted black inside with instruments connected. A simplified circuit schematics is shown in the bottom panel	27
4.15	The schematics of a single module of the power supply [18]	28
4.16	Left: Rotating switch with 3D printed holder. Right: Power supply circuit with external resistors and switch to change resistance.	28
4.17	Left: Replacement of rotating switch with a IC socket. Right: Final circuit with multiplexer and connection to Raspberry Pi	29
4.18	Sequence in which SiPM are read to avoid heating issue which causes an increase in the dark current.	30
4.20	Example for the comparison report of an annealed (for 163 hours) SiPM 161123-28 with it's non-annealed data and the relative change in dark current	31
4.19	Example for the report of a healthy SiPM 161123-17	32
5.1	Modified optical disk drive with custom 3D printed plate attached to the holder	34
5.2	(a) CAD object assembled in Autodesk Fusion 360. (b) 3D printed structures assembled with pen laser as illumination module.	34
5.3	CAD object assembled in Autodesk Fusion 360 with the illumination module.	35
5.4	LED setup used for characterization with 50Ω current limiting resistor at 5 V and 50 Omega coaxial termination resistor	36
5.5	Set-up for LED photon spread at different angles	37
5.6	LED photon spread for different increasing interval of supply voltage. Angles are in degrees and radii are in mV	37
5.7	Circuit schematics for readout of reference SiPM	38
5.8	SiPM voltage as a function of width for SiPM reverse biased at 30 V and LED voltage at 2.5 V	39
5.9	Angular absorbance of SiPM array 161123-03 at 5 V for signal width of 100 ns. Angles in degrees and radii in mV	40
5.10	Illumination module model with its cap, 3 screw holes, reference SiPM holder, filter holder and LED holder	41
5.11	3D printed illumination module with SiPM, filters and LED	41
5.12	Relative charge map for the SiPM array. SiPM 8 and 63 are missing and the small readings are due to the reflections and scattering and hence this is taken as the lower bound.	43
A.1	The compiled report of 161123-46 SiPM used in the irradiation of SiPM in the Section: 4.3	48
B.1	Dark Current map at 26 V after 266 h of annealing	50
B.2	Dark Current map at 27 V after 266 h of annealing	51
B.3	Dark Current map at 28 V after 266 h of annealing	52
B.4	Dark Current map at 29 V after 266 h of annealing	53
B.5	Dark Current map at 30 V after 266 h of annealing	54

B.6 Dark current comparison for each annealing session with non-annealed including the last 2 sessions 55

B.6 Dark current comparison for each annealing session with non-annealed including the last 2 sessions 56

B.6 Dark current comparison for each annealing session with non-annealed including the last 2 sessions 57

List of Tables

4.1	High-temperature annealing data for the SiPM 161123-07	20
4.2	Calculated voltage output for the Voltage regulator	29

Bibliography

- [1] G. Gamow. Expanding universe and the origin of elements. *Phys. Rev.*, 70:572–573, October 1946.
- [2] Mikhail Shaposhnikov. Baryon asymmetry of the universe and neutrinos. *Prog. Theor. Phys.*, 122:185–203, 2009.
- [3] Werner Bernreuther. Cp violation and baryogenesis. *CP Violation in Particle, Nuclear and Astrophysics Lecture Notes in Physics*, page 237–293, 2002.
- [4] Laurent Canetti, Marco Drewes, and Mikhail Shaposhnikov. Matter and antimatter in the universe. *New Journal of Physics*, 14(9):095012, 2012.
- [5] et al. F. Müller. A new beam polarimeter at COSY to search for electric dipole moments of charged particles. *Journal of Instrumentation*, 15(12):P12005–P12005, dec 2020.
- [6] C. Abel and et al. Measurement of the permanent electric dipole moment of the neutron. *Phys. Rev. Lett.*, 124:081803, Feb 2020.
- [7] Cosy. https://www.fz-juelich.de/ikp/ikp-4/EN/Forschung_2/Beschleuniger/_node.html. Accessed: 2020-12-15.
- [8] M. Bai, O. Felden, R. Gebel, and H.-P. May. Status of the cosy/jülich injector cyclotron julic. <https://accelconf.web.cern.ch/cyclotrons2016/papers/thp04.pdf>, 2016. Accessed: 2020-12-15.
- [9] O. Felden, M. Bai, R. Gebel, and R.Hecker. Activities for isotope sample production and radiation effect tests at julic/cosy jülich. <https://accelconf.web.cern.ch/cyclotrons2016/papers/mop18.pdf>, 2016. Accessed: 2020-12-15.
- [10] Irakli Keshelashvili (for the JEDI collaboration). Towards jedi polarimetry. http://collaborations.fz-juelich.de/ikp/jedi/public_files/proceedings/i.keshelashvili_PSTP_v1.pdf, 2015. Accessed: 2020-12-15.
- [11] D. Renker. Geiger-mode avalanche photodiodes, history, properties and problems. *Nuclear Instruments and Methods in Physics Research Section A: Accelerators, Spectrometers, Detectors and Associated Equipment*, 567(1):48 – 56, 2006. Proceedings of the 4th International Conference on New Developments in Photodetection.
- [12] SensL Technical Note. An introduction to the silicon photomultiplier. <https://www.sensl.com/downloads/ds/TN%20-%20Intro%20to%20SPM%20Tech.pdf>, 2017. Accessed: 2020-12-15.
- [13] Rongqing Hui. Photodetectors. In *Introduction to Fiber-Optic Communications*, pages 125–154. Elsevier, 2020.

- [14] E. Garutti and Yu. Musienko. Radiation damage of sipms. *Nuclear Instruments and Methods in Physics Research Section A: Accelerators, Spectrometers, Detectors and Associated Equipment*, 926:69 – 84, 2019. Silicon Photomultipliers: Technology, Characterisation and Applications.
- [15] Alexei Ulyanov, David Murphy, Joseph Mangan, Viyas Gupta, Wojciech Hajdas, Daithi de Faoite, Brian Shortt, Lorraine Hanlon, and Sheila McBreen. Radiation damage study of sensl j-series silicon photomultipliers using 101.4 mev protons. *Nuclear Instruments and Methods in Physics Research Section A: Accelerators, Spectrometers, Detectors and Associated Equipment*, 976:164203, 2020.
- [16] Michael Moll. *Radiation Damage in Silicon Particle Detectors*. PhD thesis, Hamburg University, 1999.
- [17] Laurence W. McKeen. 10 - fluoropolymers. In Laurence W. McKeen, editor, *The Effect of UV Light and Weather on Plastics and Elastomers (Third Edition)*, Plastics Design Library, pages 243 – 269. William Andrew Publishing, Boston, third edition edition, 2013.
- [18] O. Javakhishvili, I. Keshelashvili, D. Mchedlishvili, M. Gagoshidze, T. Hahnrahts, A. Kacharava, Z. Metreveli, F. Müller, T. Sefzick, D. Shergelashvili, H. Soltner, and H. Ströher. Development of a multi-channel power supply for silicon photomultipliers reading out inorganic scintillators. *Nuclear Instruments and Methods in Physics Research Section A: Accelerators, Spectrometers, Detectors and Associated Equipment*, 977:164337, 2020.
- [19] T. Tsang. Silicon photomultipliers radiation damage and recovery via high temperature annealing. *Journal of Instrumentation*, 13(10):P10019–P10019, oct 2018.
- [20] Rene Brun and Fons Rademakers. Root — an object oriented data analysis framework. *Nuclear Instruments and Methods in Physics Research Section A: Accelerators, Spectrometers, Detectors and Associated Equipment*, 389(1):81 – 86, 1997. New Computing Techniques in Physics Research V.

Acknowledgement

I would like to thank Prof. Jörg Pretz for providing me with this wonderful opportunity to work and write my thesis in the JEDI collaboration. I would also like to thank Prof. Achim Stahl for agreeing to be my second supervisor.

A very big special thanks to Dr. Irakli Keshelashvili for all the support and help during my thesis and enjoyable discussion during our lunch. This thesis would have been impossible without you.

I would like to thank all the JEDI collaboration and IKP members, especially Otari Javakhishvili for helping me throughout my thesis and answering all my questions about electronics with patience.

Needless to say, I would not be here, today, if not for my parents and my family who has constantly supported me throughout my journey since childhood. Special thanks to Vrinda Mehta and Shefali Shefali for constant support during my masters and my thesis.

I would also thank all my friends, especially Goutham Bharadwaj for all the game time we had, which always helped me to get back to work by clearing my mind after a intensive gaming session.

Subtly sliding in, thanks to corona virus for making opportunity to work from home for extended periods of time, because travelling to Jülich from Aachen everyday is a lot more difficult and unhealthy than it sounds. I would also want to extend my thanks to all those who are keeping good hygiene and following the rules properly.

Final thanks to everyone who has helped me to overcome all my endeavours till now and will be there for the future ones.

Thank you.